מכון ויצמן למדע

WEIZMANN INSTITUTE OF SCIENCE

Thesis for the degree
Doctor of Philosophy

חבור לשם קבלת התואר
דוקטור לפילוסופיה

By
Michael Stern

מאת
מיכאל שטרן

ספקטרוסקופיה אופטית של אלקטרונים וחורים באינטראקציה בבורות קוונטיים מצומדים

Optical Spectroscopy of Interacting Electrons and Holes in Coupled Quantum Wells

Regular Format

Advisor:
Prof. Israel Bar-Joseph

מנחה:
פרופ' ישראל בר-יוסף

September 2008

תשרי תשס"ט

Submitted to the Scientific Council of the
Weizmann Institute of Science
Rehovot, Israel

מוגש למועצה המדעית של
מכון ויצמן למדע
רחובות, ישראל

A mes parents et grands-parents,

A Myriam, au-delà des mots

A Elior, Avigail & Arielle, mes petits rayons de soleil

בס״ד

בן זומה אומר. איזהו חכם הלומד מכל–אדם שנאמר מכל מלמדי השכלתי כי עדותך שיחה לי: איזהו גיבור הכובש את יצירו שנאמר טוב ארך אפים ומושל ברוחו מלכד עיר: איזהו עשיר השמח בחלקו שנאמר יגיע כפיך כי תאכל אשריך וטוב לך אשריך בעולם הזה וטוב לך לעולם הבה: איזהו מכובד המכבד את הבריות שנאמר כי מכבדי אכבד ובזי יקלו:

פרקי אבות – פרק רביעי

Poser le savoir comme *l'exister* même de la créature, comme remontée, au delà de la condition, vers l'Autre qui fonde, c'est se séparer de toute une tradition philosophique qui cherchait en soi le fondement de soi, en dehors des opinions hétéronomes. Nous pensons que l'existence *pour soi* n'est pas le dernier sens du savoir, mais le remise en question de soi, le retour vers l'avant soi, en présence d'Autrui. La présence d'Autrui – hétéronomie privilégiée – ne heurte pas la liberté, mais l'investit. La honte pour soi, la présence et le désir de l'Autre, ne sont pas la négation du savoir : le savoir est leur articulation même. L'essence de la raison ne consiste pas à assurer à l'homme un fondement et des pouvoirs, mais à le mettre en question et à l'inviter à la justice.

Emmanuel Levinas, *Totalité et Infini*, Section 1-C2

Acknowledgments

I wish to express my deep gratitude to my advisor, Professor Israel Bar-Joseph, for all he taught me and helped me during these years of work. Israel offered me a unique balance of guidance and freedom, perspective and support, kindness and devotion. I wish to thank him for having confidence in my ability to switch from high-tech entrepreneurship to fundamental research.

I would like to recall the memory of dear Professor Yehoshua Levinson. Yehoshua was involved in all the theoretical parts of this research since its beginning. I feel highly fortunate to have had the opportunity to learn so much from him. Yehoshua was for me a model not only as a great scientist but also – for his kindness and generosity – as an unforgettable man.

A special acknowledgment to Dr Go Yusa, Dr Michael Rappaport and Dr Javier Groshaus has long been due. Go and Javier introduced me to the field of semiconductor spectroscopy and Michael taught me many cryogenic and experimental skills.

I thank Professors Boris Laikhtman, Shimon Levit, Schmuel Gurvitz and Nir Davidson for fruitful discussions, for their guidance and constructive comments during the years.

I wish to thank Valery Garmider for a gratifying and pleasant collaboration - Valery is a wonderful partner and a great friend- , Dr Enrico Segre whose kind patience and competence in the realm of computers was crucial to my work, and all the past and present members of Prof. Bar-Joseph's lab : Tali Dadosh, Merav Dolev, Yoav Gordin, Paulina Plochocka, Avi Guttman, Eyal Cohen-Hoshen for stimulating discussions and for always maintaining a pleasant atmosphere of work.

This research was supported by the Israeli Science Foundation, the Minerva Foundation and the Scientific Cooperation Program of the French Embassy in Tel Aviv.

Table of Contents

Abstract

Interacting electrons and holes in semiconductors may form a hydrogen like bound state, known as exciton. Its large diameter, small binding energy and strong interaction with light make it a convenient test bed for studying the effects of Coulomb interactions in many body systems. Theoretical studies have predicted a wealth of phases, gas, liquid, solid, condensate and electron-hole plasma, with thermodynamic or quantum transitions between these phases.

In the dilute limit, excitons should behave as weakly interacting Bose particles and could therefore undergo Bose Einstein condensation when their density is high enough. As excitons have a very small effective mass the critical temperature of BEC transition T_C is expected to be around 1K, six orders of magnitude higher than for atoms. This unique feature triggered intense interest and for years experimenters have tried with little success to produce BEC of excitons in the laboratory.

The Mott transition stands out as another puzzle of the field. Mott suggested in the 60's that a dense exciton system should undergo a phase transition to unbound electron-hole plasma. When the temperature (or exciton density) is low, most of the electrons and holes should be bound in excitons. As the temperature (density) increases more and more excitons are ionized, releasing free carriers. The free carriers screen the remaining excitons facilitating their ionization. Further increase of the temperature (density) leads to an avalanche ionization. This fascinating insulator to metal transition has also attracted a lot of attention in the past several decades, and there have been many attempts to observe it in semiconductors. Yet, its exact nature remained unclear.

Indirect excitons in coupled quantum wells offer a unique opportunity to revisit these long standing problems. These excitons are formed by electrons and holes that reside in different quantum wells, separated by a thin tunnel barrier. Their close proximity allows them to interact and form a bound state. This unique structure gives rise to far reaching consequences. First, the indirect exciton lifetime can be made very long, as long as microseconds, limited only by the exponentially small overlap of the electron-hole wavefunction. This allows them to establish a thermodynamic equilibrium among themselves and with the surrounding lattice. Second, these excitons are arranged as parallel dipoles, pointing to the same direction. This causes their

interaction to be repulsive, such that their total energy increases with density and generates a strong force which drives the excitons away from each other.

In this work, we studied the phase diagram of optically generated electrons and holes in coupled quantum wells. By measuring both in-plane electrical conductivity and photoluminescence properties, we found that the system undergoes an abrupt Mott transition at a critical excitation power. We measured exciton diamagnetism and showed that the transition is associated with a large increase in exciton radius, from ~20 nm below the critical density to more than 50 nm above.

We measured the temperature dependence of the transition and determined the phase diagram of the system. Interestingly, we observed a re-entrance behavior: for a given power density, an excitonic phase exists only in a limited range and it turns into electron-hole plasma below and above this range. We found that the transition is stimulated by the presence of direct excitons in one of the wells, and showed that they serve as a catalyst of the transition. Indeed, we found that in the absence of these catalysts the phase transition is gradual.

The Mott transition is also strongly manifested in the diffusion properties of the electron-hole pairs, primarily as a very large increase of the diffusion coefficient, by approximately an order of magnitude, as the system changes from bound excitons to unbound electrons and holes. We showed that the diffusion of the unbound electron hole plasma is characterized by a giant ambipolar diffusion whereas the excitonic diffusion coefficient is significantly smaller. This change in diffusion coefficient is due to exciton correlations and gives rise together with local heating at the illumination spot to a ring pattern of the photoluminescence intensity above the Mott transition. In that sense, diffusion measurements are a sensitive tool for studying pair interactions in these structures, and can distinguish very effectively between bound and unbound pairs.

תקציר

האלקטרונים והחורים באינטראקציה במוליכים-למחצה יכולים לבנות מצב קשור בדומה לאטום המימן. מצב קשור זה נקרא אקסיטון. קוטרו הגדול, אנרגית הקשר הנמוכה,, וחוזק האינטראקציה שלו עם אור הם הגורמים לו להיות בסיס טוב למחקר אינטראקציות חשמליות במערכות רב גופיות. ואכן, עבודות תיאורטיות מנבאות קיומן של פאזות שונות ומגוונות של מערכות אקסיטונים, גז, נוזל, מוצק, *BEC* ופלזמת אלקטרונים-חורים , עם מעברים תרמודינמיים וקוונטיים ביניהם.

בגבול של גז דליל, אקסיטונים אמורים להתנהג כבוזונים בעלי אינטראקציה חלשה ולכן יכולים לעבור התעבות בוזה-אינשטיין כשצפיפותם גדולה דיה. עקב מסתם האפקטיבית הנמוכה, הטמפרטורה הקריטית להתעבות בוזה-אינשטיין אמורה להיות סביב $1^{\circ}\mathrm{K}$, טמפרטורה הגבוהה בשישה סדרי גודל מאשר באטומים. תכונה מיוחדת זו עוררה עניין רב בקרב חוקרים ובמשך שנים רבות ניסיוניים ניסו לייצר *BEC* של אקסיטונים במעבדה אך עם מעט הצלחה.

שאלה אחרת בתחום קשורה למעבר מוט. בשנות הששים פרופ׳ מוט העלה את הרעיון שגז צפוף של אקסיטונים אמור לעבור מעבר פאזה לפלזמת אלקטרונים וחורים חופשיים. כשהטמפרטורה (או צפיפות האקסיטונים) נמוכה, רוב האלקטרונים והחורים נמצאים במצב קשור של אקסיטון. כשהטמפרטורה (או הצפיפות) עולה, יותר ויותר אקסיטונים עוברים יינון ומשחררים נושאי מטען חופשיים. נושאי המטען החופשיים ממסכים את יתר האקסיטונים, דבר המעודד את המשך יינונם. עליה נוספת בטמפרטורה (או בצפיפות) מובילה למפולת יינון. תופעה מרתקת זו של מעבר בין מבודד למתכת משכה אף היא את תשומת הלב בעשורים הקודמים, וניסיונות רבים נעשו על מנת לצפות בתופעה זו במוליכים למחצה, אך טבעה המדויק עדיין אינו ברור.

אקסיטונים בלתי ישירים (אב״י) בבורת קוונטיים מצומדיים נותנים את האפשרות לחקור בעיות רבות שנים אלו מחדש. אב״י נוצרים מאלקטרונים וחורים השוכנים בבורות קוונטיים שונים המופרדים ע״י מחסום פוטנציאל דק. שכנותם הקרובה נותנת להם את האפשרות לאינטראקציה וליצירת מצב קשור. למבנה ייחודי זה השלכות חשובות:

- זמן החיים של האב״י יכול להיות ארוך מאוד, עד כמה מיקרו-שניות, ומוגבל רק ע״י החפיפה הקטנה של פונקציות הגל של האלקטרון והחור. דבר זה מאפשר להם להגיע לשיווי משקל תרמודינמי בינם לבין עצמם ובינם לבין הגביש הסובב אותם.

- האב״י מסתדרים כדיפולים מקבילים המצביעים כולם לאותו הכיוון. דבר זה גורם לאינטראקציה ביניהם להיות אינטראקצית דחייה כך שהאנרגיה הכוללת של המערכת עולה עם הצפיפות ומייצר כוח חזק הדוחה אותם האחד מן השני.

בעבודה זו חקרנו את דיאגראמת הפאזות של אלקטרונים וחורים ב בורות קוונטיים מצומדיים. ע״י מדידת המוליכות במישור ומדידת תכונות הפוטולומינסנציה גילינו שהמערכת עוברת מעבר מוט חד הקורה בעצמת עירור קריטית מסוימת. מדדנו את הדיאמגנטיזם של האקסיטונים

והראנו שהמעבר קשור בהגדלה משמעותית של רדיוס האקסיטון מ-20 ננומטר מתחת לצפיפות הקריטית עד ליותר מ-50 ננומטר מעליה.

מדדנו את תלות המעבר בטמפרטורה וקבלנו דיאגראמת הפאזות של המערכת. בצורה מפתיעה ראינו שקיימת התנהגות של "מופע מחודש" (*re-entrance*): עבור עצמת אור נתונה, קיימת פאזה אקסיטונית בתחום מוגבל בלבד והיא הופכת לפלזמת אלקטרונים-חורים מעל ומתחת לתחום זה. מצאנו שהמעבר מוגבר ע"י אקסיטונים ישירים הנמצאים באחד הבורות, והראנו שהם מהווים זרז להתרחשות המעבר. ללא זרזים אלו מעבר הפאזה הינו מתון.

מעבר מוט בא לידי ביטוי בצורה חזקה גם בתכונות הדיפוזיה של זוגות האלקטרון-חור. דבר זה מתבטא בעיקר בהגדלה משמעותית של מקדם הדיפוזיה, בערך בסדר גודל, כשהמערכת עוברת ממצב של אקסיטונים למצב של אלקטרונים וחורים חופשיים. הראנו שהדיפוזיה של פלזמת אלקטרונים וחורים חופשיים מאופיינת בדיפוזיה אמביפולרית ענקית לעומת הדיפוזיה האקסיטונית הקטנה יותר בצורה משמעותית. שינוי זה במקדם הדיפוזיה נובע מקורלציות בין אקסיטונים ויחד עם חימום מקומי בנקודת ההארה גורם להופעת צורה של טבעת של עצמת הפוטולומינסנציה מעל מעבר מוט. עקב כך מדידות דיפוזיה מהוות כלי רגיש למחקר אינטראקצית זוגות במבנים אלו ויכולות להבדיל בצורה יעילה בין זוגות קשורים וחופשיים.

1. Introduction

1.1 Scientific Background

1.1.1 GaAs/AlGaAs Quantum Wells

The electronic energy-band structures of bulk GaAs have been extensively studied in the last fifty years. Like in all the III-V materials the top of the valence band occurs at the center of the Brillouin zone called Γ point. In GaAs, the conduction band edge is also found at the Γ point and therefore, its fundamental absorption edge corresponds to direct transitions.

Near the Γ point, the band structure is well described by the effective mass approximation [1]. The electron and hole effective masses can be expressed by:

$$E_{v(c)}(k) = E_{v(c)}(\Gamma) \mp \frac{\hbar^2 k^2}{2m^*_{h(e)}} \qquad (1.1)$$

where m_e^* is the effective electron mass and m_h^* can be heavy-hole or light hole effective mass. The isotropic effective mass of the electron is $m_e^* = 0.067\, m_0$, where m_0 is the electron rest mass. The effective masses of holes in bulk GaAs are also relatively isotropic near the center of the Brillouin zone. The effective mass of the heavy hole is $m_{hh}^* = 0.45\, m_0$ while the effective mass of the light hole is $m_{lh}^* = 0.08\, m_0$.

Using molecular beam epitaxy [2], it is possible to grow alternating layers of different semiconductors and to control the thickness of the different layers with a precision of around 0.2 nm. Because the difference of the lattice parameters between GaAs and $Al_xGa_{1-x}As$ is negligible [3], we can create lattice-matched heterostructures with various band offsets and tailor the barrier heights for particular applications. By sandwiching a layer of GaAs between AlGaAs, a type I quantum well (QW) is formed in the growth direction (z-direction).

The electrons and holes in this GaAs layer are confined in a one-dimensional potential well. This confinement has a significant effect on the energy states which become discrete in the z-direction. The energy of the ground state of an idealized quantum well is a function of the quantum well thickness, the potential width and the

effective mass [1]. As a consequence, the introduction of a band gap discontinuity in the form of quantum wells modifies the band structure. The confinement causes a removal of valence band degeneracy at k=0, and an energy gap is formed between the heavy and light hole subbands.

Moreover, the heavy and light hole masses are anisotropic in quantum wells. The dispersion equation gives the following expression for in-plane (x-y plane, ∥) and perpendicular (z-direction , ⊥) hole masses:

$$\begin{aligned} m_{hh,\perp} &= \frac{1}{\gamma_1 - 2\gamma_2} m_0 \qquad m_{lh,\perp} = \frac{1}{\gamma_1 + \gamma_2} m_0 \\ m_{hh,//} &= \frac{1}{\gamma_1 + \gamma_2} m_0 \qquad m_{lh,//} = \frac{1}{\gamma_1 - \gamma_2} m_0 \end{aligned} \tag{1.2}$$

where $\gamma_1 = 7.10$ and $\gamma_2 = 2.02$ are the Luttinger parameters and m_0 is the electron mass [4].

1.1.2 Wannier Excitons

When GaAs is illuminated with near band-gap light, electron-hole pairs are created. If the electron and hole were non-interacting, only photons with energy above E_g would be absorbed. However, the Coulomb interaction between electrons and holes greatly modifies this picture. The electron-hole attraction gives rise to a bound state called exciton [5-7].

Because the exciton is weakly bound and spreads over many lattice sites, the electron hole interaction is screened by the dielectric constant ($\varepsilon \approx 12.9$ in GaAs). The exciton Hamiltonian can be written as:

$$\left[\frac{p_e^2}{2m_e^*} + \frac{p_h^2}{2m_h^*} - \frac{e^2}{\varepsilon |r_e - r_h|} \right] \Psi(r_e, r_h) = (E - E_g) \Psi(r_e, r_h) \tag{1.3}$$

It is convenient to rewrite this Hamiltonian as function of $r = r_e - r_h$ and of R the center of mass coordinate:

$$\left[\frac{P^2}{2(m_e^* + m_h^*)} + \frac{p^2}{2\mu} - \frac{e^2}{\varepsilon r} \right] \Psi(r, R) = (E - E_g) \Psi(r, R) \tag{1.4}$$

with $P = -i\hbar \partial / \partial R$, $p = -i\hbar \partial / \partial r$ and μ is the reduced mass of the electron-hole pair.

Since the Hamiltonian does not depend on R, P is a good quantum number and therefore it is possible to write

$$\Psi(r,R) = \frac{1}{\sqrt{\Omega}}\exp(iK.R)\varphi(r) \qquad (1.5)$$

where Ω is the volume of the crystal.

By writing $E = E_g + \frac{\hbar^2 K^2}{2(m_e^* + m_h^*)} + \eta$, we finally obtain:

$$\left[\frac{p^2}{2\mu} - \frac{e^2}{\varepsilon r}\right]\varphi(r) = \eta\varphi(r) \qquad (1.6)$$

whose ground state wavefunction is the well-known 1S hydrogenic wavefunction.

In GaAs, the excitonic Rydberg is given by $Ry = \frac{\mu e^4}{2\varepsilon^2\hbar^2}$ ~ 5 meV and the exciton Bohr radius is $a_B = \frac{\hbar^2\varepsilon}{\mu e^2}$ ~ 100 Å.

1.1.3 Excitons in quantum wells

Bound and continuum states of excitons in 3D are basically similar to those found in the hydrogen atom discussed in general quantum mechanics books. The theory of excitons is similar in strictly two dimensional limit, where the thickness in the z-direction is assumed to be zero. In this limit 2D case [8], the energy levels are given by:

$$E_n^{2D} = -\frac{Ry}{\left(n - \frac{1}{2}\right)^2} \qquad (1.7)$$

Therefore, the binding energy of excitons in 2D is four times that in the 3D case.

For finite thickness quantum well structures, the situation is more complex and an analytical solution cannot be found [9-10]. For simplicity, we will assume that both materials have the same electron and hole effective mass. The Hamiltonian can be generalized to:

$$H = \frac{p_e^2}{2m_e^*} + \frac{p_{h,\perp}^2}{2m_{hh/lh,\perp}^*} + \frac{p_{z_h}^2}{2m_{hh/lh,//}^*} - \frac{e^2}{\varepsilon|r_e - r_h|} + V_e Y\left[z_e^2 - \frac{L^2}{4}\right] + V_h Y\left[z_h^2 - \frac{L^2}{4}\right] \qquad (1.8)$$

where Y is the step function, L is the quantum well thickness and $V_{e(h)}$ the barrier potential for electrons (holes).

It is convenient to rewrite this Hamiltonian as function of $R_\perp = \frac{m_e^* \rho_e + m_{hh/lh,\perp}^* \rho_h}{m_e^* + m_{hh/lh,\perp}^*}$

and $\rho = \rho_e - \rho_h$ where $\rho_{e(h)}$ are the in-plane coordinates of the electron (hole).

$$H = \frac{P_\perp^2}{2(m_e^* + m_{hh/lh,\perp}^*)} + \frac{p_\perp^2}{2\mu_{hh/lh}} - \frac{e^2}{\varepsilon\sqrt{\rho^2 + (z_e - z_h)^2}} + V_e Y\left[z_e^2 - \frac{L^2}{4}\right] + V_h Y\left[z_h^2 - \frac{L^2}{4}\right] + \frac{p_{ze}^2}{2m_e^*} + \frac{p_{zh}^2}{2m_{hh/lh,//}^*} \tag{1.9}$$

with $\mu_{hh/lh}$ the reduced mass of the heavy/light hole exciton.

Since the Hamiltonian does not depend on $R_\perp$, $P_\perp$ is a good quantum number and therefore it is possible to write

$$\Psi(r_e, r_h) = \frac{1}{\sqrt{S}} \exp(iK_\perp . R_\perp) \varphi(z_e, z_h, \rho) \tag{1.10}$$

The equation (1.10) is then solved by using a variational procedure using the following trial wavefunction:

$$\varphi(z_e, z_h, \rho) = N\chi_{1,e}(z_e)\chi_{1,h}(z_h) \exp\left[-\frac{1}{\lambda}\sqrt{\rho^2 + (z_e - z_h)^2}\right] \tag{1.11}$$

where $\chi_{1,e}$, $\chi_{1,h}$ are the ground state eigenfunctions of the electron/hole quantum wells and λ the variational parameter. The typical value of the exciton binding energy in a quantum well is ~10 meV [10].

1.1.4 Indirect Excitons in Coupled Quantum wells

The system we will study in this thesis is formed by two GaAs quantum wells separated by a thin AlGaAs barrier. An external electric field is applied in the z-direction perpendicular to the QWs. By that way, the electrons initially created in one of the well can tunnel to the second well and form a two dimensional gas of spatially indirect excitons. The Figure 1a illustrates the potential profile along the growth direction.

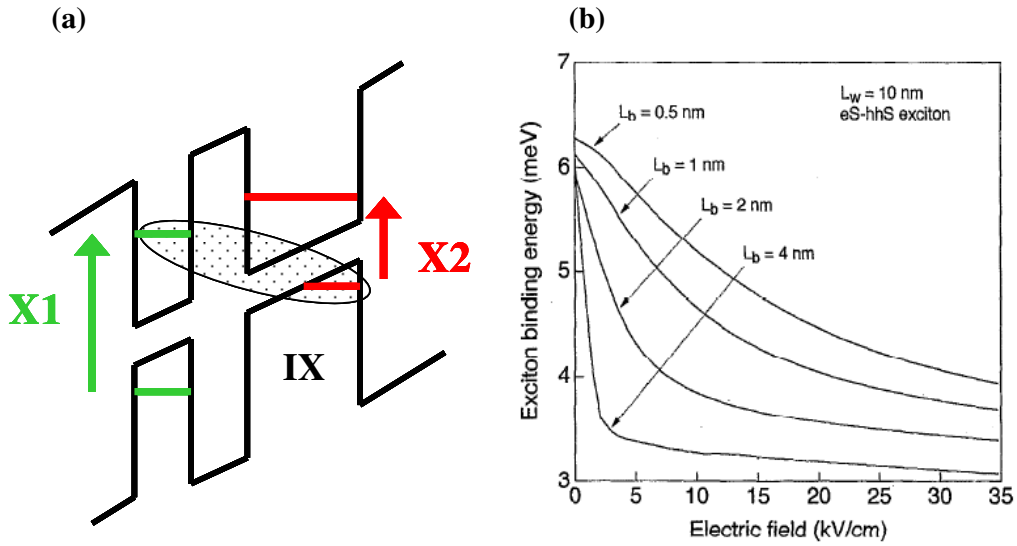

FIG. 1 - **(a)** The energy band diagram of asymmetric coupled quantum wells under perpendicular applied electric field. X1 (in green) corresponds to the exciton in narrow well, X2 (in red) to the exciton in the wide well and IX (black ellipse) to the indirect exciton. The electric field separates by several meV the Xs and IX photoluminescence energies. **(b)** Calculated binding energies using variational method as function of applied electric field. The well width is 10 nm. The barrier width is varied from 0.5 to 4 nm. After reference [11].

The close proximity of the electron and hole allows them to interact and form a bound state. The energy levels, binding energy and Bohr radius of indirect excitons can be calculated by different methods [11-14] using the following Hamiltonian expressed directly in the relative and center of mass coordinates :

$$H = \frac{P_{\perp}^2}{2(m_e^* + m_{hh/lh,\perp}^*)} + \frac{p_{\perp}^2}{2\mu_{hh/lh}} - \frac{e^2}{\varepsilon\sqrt{\rho^2 + (z_e - z_h)^2}} + V_e(z_e) + V_h(z_h) \\ - eF(z_e - z_h) + \frac{p_{ze}^2}{2m_e^*} + \frac{p_{zh}^2}{2m_{hh/lh,//}^*} \qquad (1.12)$$

The Hamiltonian can be solved using a variational trial wavefunction similar to that used for direct excitons in single quantum wells (1.11). A typical value of the binding energy of indirect excitons is ~ 4 meV under an applied electric field of ~ 20 kV/cm as shown on Fig. 1b.

One of the main properties that distinguish indirect excitons is their long lifetime. The radiative recombination rate of excitons can be calculated according to the Fermi golden rule when the interaction with the photon is given by $-e/m_0\vec{A}.\vec{p}_e$ where $\vec{A}$ is the vector potential of the light in the sample and $\overrightarrow{p_e}$ is the electron momentum operator. The lifetime of excitons can be written as:

$$\frac{1}{\tau_{IX}} = \frac{4\pi^2 e^2}{\varepsilon m_0^2 \Omega} \sum_{q,s} \frac{1}{\omega_q} \left| \left\langle 0 \left| \vec{\lambda}_{q,s} \exp[-i\vec{q}.\vec{r}_e] \vec{p}_e \right| \Psi_{\vec{K}} \right\rangle \right|^2 \delta(E - \hbar\omega_q) \qquad (1.13)$$

where $\vec{\lambda}_{q,s}$ and ω_q are respectively the polarization vector and the frequency of the photon with the wavevector q and polarization mode *s* and Ψ_K the wavefunction of an exciton with wavevector $\overrightarrow{K}$. It can be shown that the recombination rate is proportional to the electron-hole overlap integral [14] which can be written as:

$$\Sigma = \left| \int \chi_{1,e}(z_e).\chi_{2,h}(z_h)\delta(z_e - z_h)dz_e dz_h \right|^2 \qquad (1.14)$$

Therefore, indirect exciton*s* have a much longer lifetime than direct excitons due to the spatial separation of electrons and holes in different quantum wells. When the applied electric field is raised, the wavefunction confinement reduces the overlap integral, thus increasing the radiative lifetime by several orders of magnitude. Figure 2a shows the oscillator strength according to calculations of Ref. [14] for 8-nm GaAs coupled quantum wells (CQW) separated by a 4-nm AlGaAs barrier. In Fig 2b, we show the ground state wavefunctions of electrons and holes at different electric fields.

In the 90's, several groups performed nanosecond time-resolved photoluminescence measurements and observed indirect excitons with lifetime of ~ 200 ns [15-17]. The dependence of the lifetime on the applied electric field was demonstrated experimentally by Alexandrou *et al*. as shown on Fig. 2c.

It should be noted that the indirect exciton lifetime is much longer than the relaxation time with the thermal bath of the lattice – typically around 1ns - and the exciton

formation time [18-24] and thus allows establishing a thermodynamic equilibrium even at low temperature.

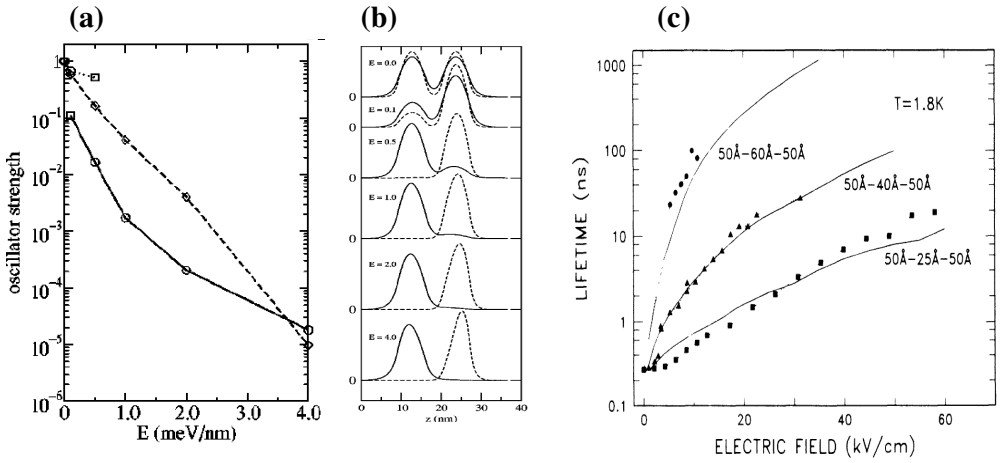

FIG. 2- **(a)** The calculated oscillator strengths for two different CQW structures as function of the applied electric field. **(b)** Ground state wavefunction for 8-nm GaAs CQW separated by a 4-nm AlGaAs barrier and for different values of the applied electric field. The solid line is the electron wavefunction while the dashed line shows the hole wavefunction. After reference [14]. **(c)** Lifetime of indirect excitons as function of the applied electric field. After reference [17].

Moreover, this long lifetime gives rise to a large diffusion length of the order of several micrometers, $l \sim \sqrt{D\tau_{IX}}$, where D is the diffusion coefficient of the excitons. This length scale is conveniently accessed using optical techniques, and allows performing detailed studies of exciton flow by means of optical spectroscopy. Indeed, in the last couple of years, several groups performed spatially resolved photoluminescence (PL) experiments of indirect excitons in order to determine their diffusion properties [25-27].

In the case of purely diffusive process, the exciton diffusion is described by the following equation:

$$\frac{\partial n_{IX}}{\partial t} = D\nabla^2 n_{IX} - \frac{n_{IX}}{\tau_{IX}} + G(r,t) \qquad (1.15)$$

where $G(r,t) = n_0 \exp\left[-\frac{r^2}{2\vartheta^2}\right]\delta(t)$ is the generation rate of excitons, n_0 is the initial density of excitons at $r = 0$, and ϑ is the initial width of the exciton profile. It is easy to show that the solution of Eq. (1.15) is given by:

$$n_{IX}(r,t) = \frac{n_0 \vartheta^2}{\vartheta^2 + 4Dt} \exp\left[-\frac{r^2}{2\vartheta^2 + 4Dt} - \frac{t}{\tau_{IX}} \right] \qquad (1.16)$$

which implies that the variance of the exciton profile increases linearly with time following $\sigma^2 = 2Dt + \vartheta^2$. Voros *et al.* used this property to measure the diffusion constant of the excitons with time-resolved luminescence [27]. In Fig. 3a, we show a series of temporally resolved exciton profile. The data in the figure are fits to Gaussian distributions. In Fig. 3b, the time dependence of the variance allows the precise determination of the diffusion coefficients in different coupled quantum wells.

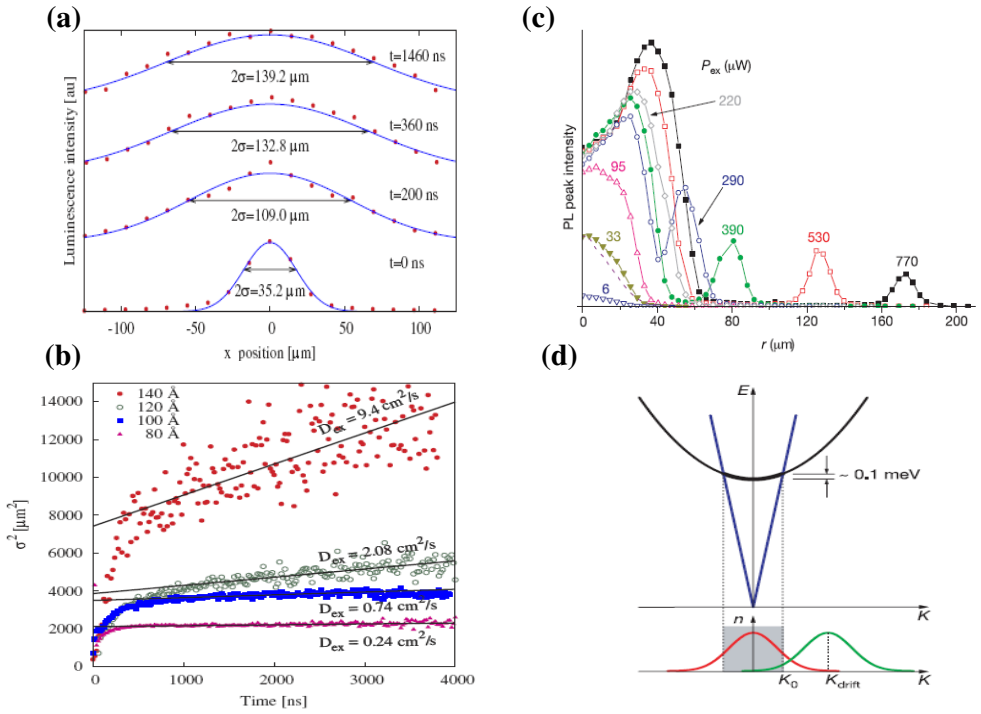

FIG. 3- **(a)** Expansion of the exciton cloud at different time after the excitation. **(b)** Measured variance versus time. The straight lines represent the linear fit, when the expansion is purely diffusive. After reference [27]. **(c)** Radial dependence of the indirect exciton photoluminescence under cw HeNe illumination at T=1.8K and at different excitation power. After reference [25]. **(d)** The reduction of PL intensity for excitons in motion. Energy diagram for the exciton (in black) and photon (in blue) showing the radiative zone where the excitons can directly recombine to photons. Schematic momentum distribution of excitons without (red) and with (green) average velocity.

An interesting observation in these experiments (Fig. 3c) is the appearance of two photoluminescence rings around the excitation spot [25-26].

The external ring, which was originally thought of as due to a degenerate exciton gas, was later shown to be due to recombination of excess free carriers in the quantum

well [28-29]. An excess of holes in the quantum well is formed under the laser excitation spot as the trapping rate of holes in the quantum well is larger than the trapping rate of electrons. The illumination spot is surrounded by a sea of electrons coming from leakage currents which recombine with the diffusing holes. A sharp luminescence ring is formed at the boundary between the two regions of opposite charge.

The inner ring was attributed to enhanced luminescence of excitons as they cool down while diffusing away from the hot excitation spot [25]. As a matter of fact, the PL intensity of an exciton system is due to cold excitons, which have a center of mass momentum smaller than the photon momentum as shown on Fig. 3d. Higher momentum excitons need to slow down before they can recombine through photon emission. The trade-off between cooling, which enhances the PL, and diffusion, which decreases it, gives a maximum at the ring location. A detailed hydrodynamic model was proposed to describe this process, and predicted a high degeneracy of the exciton gas at the ring location [30-31]. This was perceived as a step towards Bose Einstein condensation, and an optical trap which is based on this effect was demonstrated [32-33].

1.1.5 The phase diagram of a dense and cold exciton gas

The properties of a cold and dense gas of excitons have been studied intensively both experimentally and theoretically in the past decade. Theoretical studies have predicted a wealth of phases, gas, liquid, solid, condensate and electron-hole plasma, with thermodynamic or quantum transitions between these phases.

In the dilute limit, excitons should behave as weakly interacting Bose particles and could therefore undergo Bose Einstein condensation (BEC) when their density is high enough. As excitons have a very small effective mass the critical temperature of BEC transition T_C is expected to be relatively high. This unique feature triggered intense interest and for years experimenters have tried with little success to produce BEC of excitons in the laboratory.

A dense exciton system should also undergo a phase transition to unbound electron-hole plasma called Mott transition. As the density increases, more and more excitons are ionized, releasing free carriers. The free carriers screen the remaining excitons facilitating their ionization. Further increase of the density should lead to avalanche

ionization. There have been many attempts to observe the Mott transition in semiconductors. Yet, its exact nature remained unclear.

In the following sections we shall describe in more details these two transitions.

BEC of excitons

From a fundamental viewpoint, excitons are spatially extended composite particles made of loosely-bound fermions. In a second quantization formulation, the annihilation operator of an exciton can be written in terms of electron hole operators:

$$A_p = \sum_k \phi_k \times a_{e,\frac{p}{2}+k} a_{h,\frac{p}{2}-k} \qquad (1.17)$$

where Φ_k is the Fourier transform of the hydrogenic wavefunction.

The commutator of two exciton operators can be written as [34]:

$$\left[A_p, A_{p'}^+\right] = \delta_{p,p'} + \sum_q \left\{ \phi^*_{q-\frac{p'}{2}} \phi_{q-\frac{p}{2}} a^+_{e,q-Q} a_{e,q+Q} + \phi^*_{\frac{p'}{2}-q} \phi_{\frac{p}{2}-q} a^+_{h,q-Q} a_{h,q+Q} \right\} \qquad (1.18)$$

with $Q=p'-p$. It is easy to show that the right-hand side of this equation is of the order of $n*a_B^3$ where n is the density of excitons and therefore, in the dilute limit ($na_B^3 << 1$), excitons should behave as weakly interacting Bose particles. However, when n approaches the level where the inter-particle spacing becomes comparable to a_B a crossover from Bose to Fermi statistics occurs. Therefore, excitons no longer retain their boson-like character at high densities.

Three dimensional Bose gas at low temperature undergoes the Bose-Einstein condensation (BEC) which is the macroscopic occupation of the ground state of the gas [35-37]. The theoretical critical temperature of the BEC transition T_C is given by the formula (1.19).

$$T_C^{3D} = 0.527 \times \frac{2\pi\hbar^2}{Mk_B} n^{2/3} \qquad (1.19)$$

where M is the particle mass.

As excitons have a very small effective mass ($M \sim 0.15\ m_0$), they should exhibit bosonic features at relatively high temperature. Due to the small effective mass of excitons, the critical temperature of BEC transition T_C is expected to be around 2K for an exciton density of ~10^{15} cm^{-3}.

Since the 70's, there have been many theoretical and experimental attempts to prove that exciton gas exhibits the Bose Einstein condensation and/or superfluidity [38-68].

Cooling semiconductor lattice well below 1K is commonly achieved in He refrigerators. However, the temperature of excitons can in practice considerably exceed that of the semiconductor lattice. As a matter of fact, the typical exciton lifetime in GaAs is of the order of 100 ps whereas their relaxation time with the thermal bath of the lattice - which is mainly due to acoustical phonon scattering at low temperature- exceeds 1ns.

The focus of the experimental efforts in the early days was therefore on indirect-gap semiconductors like germanium, cuprate chloride and cuprate oxide whose exciton ground states are optically inactive and have a very long lifetime [42-49]. Nevertheless, the exciton density obtained in these systems did not reach the level required to achieve a Bose Einstein condensate gas [48-49].

In two dimensions the situation is more complicated in Bose liquids in general and especially in exciton liquid. It should be noted that in a strictly two dimensional system, an ideal BEC cannot occur due to the constant density of state in 2D. However, this result is true only for a system confined by rigid boundaries. If a system is confined by a spatially varying potential, the density of state is modified and a BEC can theoretically still occur [69-70].

There are other theoretical obstacles for a Bose Einstein condensate in two dimensions. In general, long wave length fluctuations are more important and the corrections to the mean field theory are more dominant in two dimensions than in three dimensions. The phase fluctuations destroy the long range order and the Bose Einstein condensation could not occur theoretically at finite temperatures. However, it was shown [71] that even in two dimensions the phase transition to superfluidity can take place.

These bosonic features should appear when the chemical potential ζ is small compared to the temperature. According to the relation between the concentration and chemical potential for Bose statistics,

$$\exp\left[-\frac{\pi\hbar^2 n}{2Mk_B T}\right] = 1 - \exp\left[\frac{\varsigma}{k_B T}\right] \qquad (1.20)$$

the degeneracy parameter is $\frac{\pi\hbar^2 n}{2Mk_B T} = \frac{\pi n}{k_T^2}$ where k_T is the thermal wave vector. For example, at $n \sim 10^{10}\,\mathrm{cm}^{-2}$ and $T = 2$ K this parameter is ~1.5.

The bosonic properties of indirect exciton gas have been studied intensively both experimentally and theoretically in the past several decades [55-65] and there have been numerous claims of observation of BEC of excitons or excitonic superfluidity. These reports raised, however, an intensive debate as each of the experimental claims could in fact be subject to more than one interpretation.

In 1990, Fukuzawa *et al*. observed a sharp reduction of the photoluminescence linewidth of indirect excitons at a certain critical temperature and under the influence of an electric field. They attributed such a narrowing to a phase transition of the exciton system into an ordered state [55]. Nevertheless, this striking temperature dependence of the luminescence linewidth and peak position was finally explained quantitatively by Kash *et al*. [56]. It was noted that the interface roughness of the quantum wells leads to a position-dependent exciton energy. Below a certain temperature, excitons are trapped in valleys as the typical time for an exciton to get out of these valleys is of the same order of magnitude as the indirect exciton lifetime. This metastable trapping occurs below a threshold temperature and is manifested by a constant luminescence of indirect excitons under the said temperature.

More recently, Butov *et al*. spatially-resolved the photoluminescence of direct and indirect excitons of uniformly illuminated CQWs and observed a strongly localized photoluminescence [62]. They first attributed it to condensation of a degenerate exciton gas in a natural trap formed by fluctuations of the quantum well thickness. Nevertheless, new observations showed that quantum well thickness fluctuations are unlikely to be the cause of the collection of indirect excitons. A weak photocurrent was observed at the trap center and it was shown that the indirect exciton cloud is formed by a continuous formation of these excitons through photoinduced carrier transport via a defect [64].

Mott Transition of excitons

Another interesting open question is the possibility of the Mott transition [72-73]. At sufficiently high densities, screening of the electron-hole coulomb attraction prevents the binding of electron-hole pairs, and the insulating exciton gas can undergo a Mott transition to a conducting electron-hole plasma. Mott suggested that there has to be a first-order phase transition between metallic and insulating states of the electron-hole gas. When the temperature (density) is low, most of the electrons and the holes are bound in excitons. With an increase of the temperature (density) more and more

excitons are ionized, releasing free carriers. The free carriers screen the remaining excitons, facilitating their ionization. Further increase of the temperature (density) leads to an avalanche ionization, i.e., to a sharp transition to a free-carrier state.

The transition comes about due to screening out of the Coulomb interaction and therefore occurs when $l \sim a_B$ where l is the screening length, which enters into the screened Coulomb potential (Yukawa). A back off the envelope estimate of the density of the transition can be given using the Debye screening formula: the exciton is screened when

$$l^2 = \frac{\varepsilon k_B T}{e^2 n_e} \sim a_B^2 \tag{1.21}$$

where n_e is the 3-D free electron-hole pair density. Therefore, at a temperature of around 2K, the Mott transition should occur for an electron-hole density of $\sim 10^{15}\,\mathrm{cm}^{-3}$.

The same argument can be applied to two dimensional structures. In that case, the screening length is given by [74]:

$$l = \frac{2\varepsilon k_B T}{e^2 n_e} \sim a_B \tag{1.22}$$

where n_e is the 2-D free electron-hole pair density.

If we assume that exciton and electron-hole gases are non degenerated and non interacting, it is possible to use Saha equation to determine the corresponding exciton density n_X by:

$$\frac{n_e^2}{n_X} = \frac{\rho_e \rho_h}{\rho_x} k_B T \exp(-\frac{E_B}{k_B T}) \tag{1.23}$$

where ρ_e, ρ_h, and ρ_x are the density of states of the electrons, holes and excitons and E_B is the binding energy of the exciton. For $T = 2$ K we get $n \sim 10^{10}$ cm^{-2}.

There were several attempts to test Mott prediction experimentally in semiconductors. An evidence for the Mott transition would be an abrupt ionization at some critical pair concentration, which will manifest itself in the photoluminescence signal. The exciton photoluminescence was measured as function of the pump excitation power. However, the exact nature of the Mott transition is still not clear. In some experiments, the change in the density of excitons due to the ionization was reported

to be continuous [75-78] while in the other papers [79-82] the change was abrupt as shown on Fig. 4a. In two-dimensions there is no experimental evidence for a thermodynamic phase transition of the exciton gas [83]. Rather, a gradual change in the optical properties has been observed as shown on Fig. 4b.

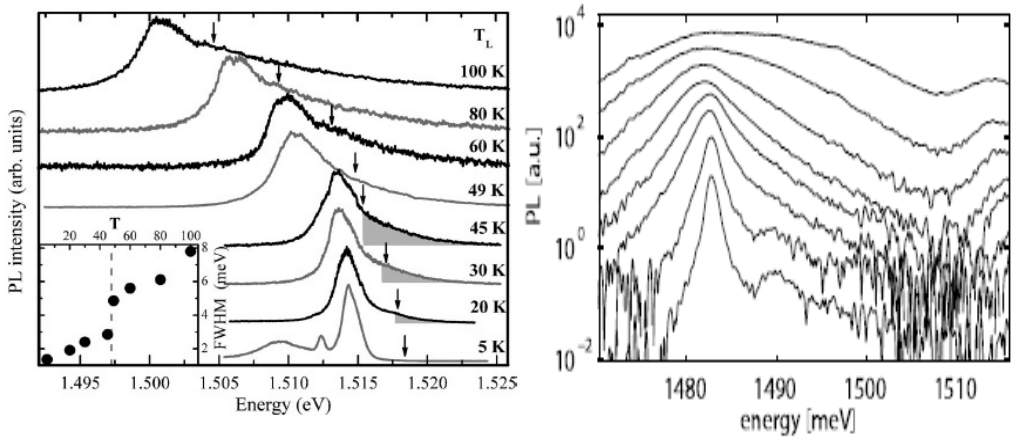

FIG. 4 – **(a)** PL spectra recorded 1.8 ns after an initial pulse excitation on bulk GaAs for different lattice temperature. The shadowed regions show the free electron-hole luminescence. **Inset** : FWHM of the whole luminescence band. After reference [82]. **(b)** Spectra of an 80 Å InGaAs/GaAs QW for different excitation powers. The carrier density is increased from lower to upper curves from 1.6 10^{9} to 6.2 10^{11} cm^{-2}. After reference [83].

At the same time, conflicting theoretical predictions have been recently published [84-89], with some predicting an abrupt phase transition at a critical temperature or density [87], while others arguing that there should be a gradual transition [89].

The approach of Ben Tabou and Laikhtman [87] was to calculate - in the mean field approximation - the free energy of a system which consists of free electrons and holes and excitons. To carry out this calculation, they show that the energy of a gas formed of N_X excitons can be written in the mean field approximation as:

$$E_X = \sum_P \left(\frac{P^2}{2M} - E_B \right) n_P + \frac{U_0}{2S} N_X^2 \qquad (1.24)$$

where $U_0 = 5U_d / 4 + V_x$, U_d is the direct interaction matrix element and V_x is the exchange interaction. These matrix elements depend on the structure geometry and were calculated in [87].

On the other hand, the energy of the electron hole plasma in Hartree Fock approximation can be written as:

$$E_{eh} = \sum_{p_e} \frac{p_e^2}{2m_e^*} n_{p_e} + \sum_{p_h} \frac{p_h^2}{2m_{h,//}^*} n_{p_h} + \frac{U_{ee} + U_{eh}}{2S} N_e^2 + \frac{U_{hh} + U_{eh}}{2S} N_h^2 \qquad (1.25)$$

where U_{ij} are the $q = 0$ value of the Fourier transform of the Coulomb interaction between particles as calculated in [87] .

The free energy of the system is then calculated using the thermodynamic perturbation theory, where the free energy of a gas with Hamiltonian $H_0 + H_1$ is given by $F = F_0 + \langle H_1 \rangle$ and where H_0 is the Hamiltonian of the ideal gas.

The equilibrium free carrier concentrations are then given by writing the equality of the chemical potentials.

$$\begin{aligned} &\varsigma_e + \varsigma_h = \varsigma_X \\ &\varsigma_e^0 + \varsigma_h^0 + (U_{ee} + 2U_{eh} + U_{hh}) n_{e-h} = \varsigma_X^0 + n_X \left(U_0 + \frac{\partial E_B}{\partial n_e} + \frac{\partial E_B}{\partial n_h} \right) \end{aligned} \qquad (1.26)$$

$\varsigma_e^0, \varsigma_h^0, \varsigma_X^0$ are the chemical potentials of ideal gases given in all textbooks of statistical physics. The derivatives of the binding energy enter in this equation because of the screening which has been calculated using dynamical screening or simple static Thomas Fermi screening.

The results of these calculations show that the Mott transition is an abrupt transition with a jump in the free carrier concentration which can reach four orders of magnitude as shown on Fig. 5a.

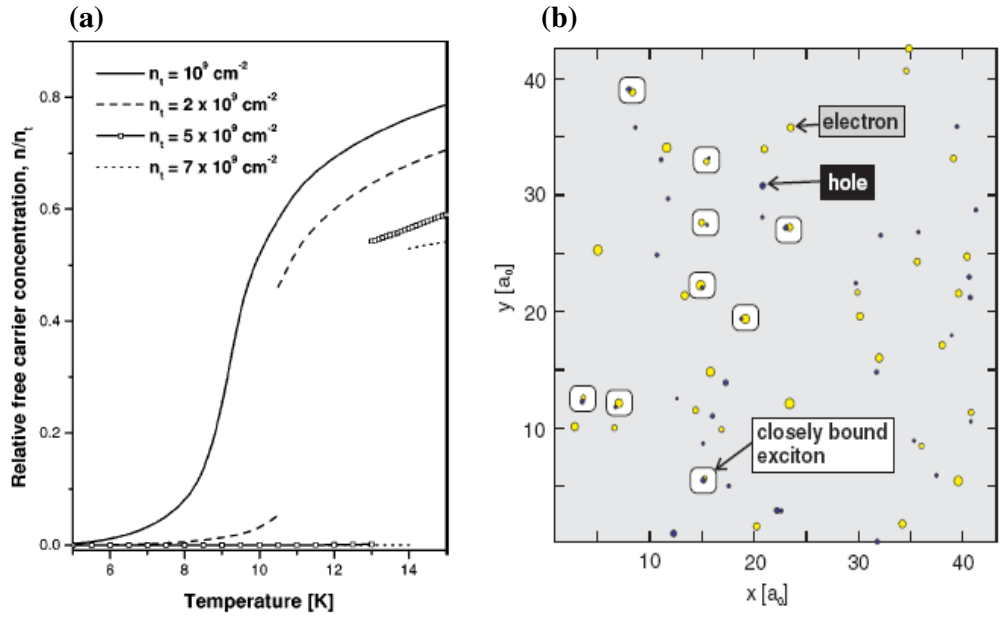

FIG. 5 – **(a)** The temperature dependence of the free carrier concentration in coupled quantum wells for different total electron-hole pair concentration. Below the critical point, the dependence is smooth. At large density, the jump of the free-carrier concentration can reach four orders of magnitude. After reference [87] **(b)** Monte Carlo simulation showing the segregation between excitonic and free electron hole regions. After reference [89]

On the other hand, Koch *et al.* used a completely different approach beyond the mean field approximation [89]. Using two different techniques namely a dynamical density matrix approach and a path integral Monte Carlo analysis, they studied the evolution as function of electron-hole pair density of the electron-hole pair correlation function defined by:

$$g(r,t) = \left\langle \Psi_e^+(r,t)\Psi_e(r,t)\Psi_h^+(r=0,t)\Psi_h(r=0,t) \right\rangle \quad (1.27)$$

where $\Psi_e(r,t)$ annihilates an electron at position r and time t. This function determines the conditional probability density to find an electron at distance r while the hole is located at $r=0$. It is possible to separate the correlation function into its Hartree Fock part and the correlated contribution:

$$g(r,t) = g_{HF}(r,t) + \delta g(r,t) \quad (1.28)$$

Contrary to the original Mott scenario where the bound pairs become more weakly bound for increasing density due to the increasing screening effects, they observed - using both methods - that the width of the correlation function becomes narrower as

the ionization density is approached indicating that the remaining pairs are even more strongly correlated than a stand-alone single exciton.

At the same time, the overall magnitude of the correlation function decreases continuously with increased carrier density. This indicates that the number of bound excitons in the system decreases continuously until an ionized plasma is formed.

The exciton binding energy depends weakly on density because the excitons can move without restrictions contrary to other metal-insulator transitions where the electrons move but the ions are arranged in lattice.

In the Monte Carlo analysis, it was even possible to show that the system finds configurations where bound pairs are sufficiently far away from surrounding carriers that screening effects are avoided as shown on Fig. 5b.

1.2 Summary of the results

In this work, we studied the properties of interacting electrons and holes in coupled quantum wells. The main findings of this PhD work are the following:

- We report the observation of the Mott transition in this system. The transition is manifested as an abrupt change in the conductivity and in the photoluminescence linewidth and peak energy at some critical power density and temperature. The transition is extremely abrupt and can not be resolved within our power resolution.
- By measuring the exciton diamagnetism, we show that the transition is accompanied by a substantial change of exciton size, from ~20nm below the critical density to more than 50 nm above. Two regimes of diamagnetism are clearly observed, with a sharp boundary between a phase of bound excitons and a phase of unbound electron-hole pairs.
- We measured the temperature dependence of the transition and determined the phase diagram of the system. Interestingly, we observe a re-entrance behavior: for a given power density, an excitonic phase exists only in a limited range and it turns into electron-hole plasma below and above this range. To understand this behavior, we constructed a phenomenological model which takes into account the changes in entropy of the system.

- We find that the transition is stimulated by the presence of direct excitons in one of the wells, and show that they serve as a catalyst of the transition. Indeed, we find that in the absence of these catalysts the phase transition is gradual.
- We show the role of correlations in the exciton-exciton interaction energy and its consequences in the density dependent blueshift of the indirect exciton photoluminescence line.
- We study the diffusion process as the system undergoes a Mott transition. We show that the transition is strongly manifested in the diffusion properties, primarily as a very large increase of the diffusion coefficient, by approximately an order of magnitude, as the system changes from bound excitons to unbound electrons and holes.
- We show that this change in diffusion coefficient together with local heating at the illumination spot give rise to a ring pattern of the PL intensity at the Mott transition. Our work disproof some previous claims that the ring formation is due to a change of the excitonic diffusion near the BEC transition and can be used to form an excitonic trap. Rather, we show that when the PL ring is observed the system consists of unbound electrons and holes, way above the Mott transition.

2. Main Results

In this section, the most important findings of this PhD work are presented. The first chapter presents quickly the experimental setup, focuses on the role of the applied electric field and on the measure of exciton lifetime and temperature. The second chapter describes our results concerning the observation of the Mott transition of excitons. In the third chapter, we show the role of correlations in the exciton-exciton interaction and its major consequences in terms of diffusion of electron-hole pairs below and above the Mott transition.

2.1 Indirect excitons in coupled quantum wells

2.1.1 Experimental setup

The samples that we investigated are $n-i-n$ structures grown by molecular beam epitaxy on semi-insulating GaAs substrate. The i-region consists of two GaAs quantum wells separated by a $Al_{0.28}Ga_{0.72}As$ barrier and surrounded by two $Al_{0.28}Ga_{0.72}As$ spacer layers. We studied two different systems: a symmetric one consisting of two identical QWs (8 nm) separated by a 4-nm barrier and an asymmetric system consisting of QWs of different widths (7/10 nm) separated by a 5-nm barrier. An electric field *F* was applied between the highly conducting *n* layers in a direction perpendicular to the QWs (Fig. 6).

We found that the leakage current through the system is suppressed by 2-3 orders of magnitude by etching most of the top n layer, leaving a thin resistive layer. The resulting dark current at 24 kV/cm is below 50 pA.

The samples were excited using a Ti:Sapphire laser with energy $E_L \leq 1580$ meV slightly above the GaAs QW gap. The fact that the excitation energy is well below the $Al_{0.28}Ga_{0.72}As$ gap substantially reduces the leakage current and does not create excess free carriers in the quantum wells [28]: a typical value of the photo-leakage is 250 μA/cm^2 at excitation power of 1W/cm^2 and electric field of 24 kV/cm.

In the case of the asymmetric quantum well samples, it is possible to select the excitation energy E_L to be above or below the narrow well gap energy E_{NW}. At

$E_L < E_{NW}$, electrons and holes are excited in the wide well only. The electrons quickly tunnel into the narrow well and at steady state one gets nearly complete charge separation: the electrons reside in the narrow well while the holes are in the wide well. This is changed when $E_L > E_{NW}$, when electrons and holes are created at both wells. Here also the electrons would tunnel into the narrow well. However, the tunneling time of the holes is much longer and we get a population of holes trapped at the narrow well. As a consequence we get a mixture of two types of excitons: indirect and direct ones, the latter being formed between electrons and holes in the narrow well. We shall see that this difference has far reaching implications on the nature of the transitions.

2.1.2 Influence of the Electric Field

The applied electric field has several effects on the coupled quantum well system:

1. In the absence of the electric field *F*, the optical transitions with lowest energy are the direct exciton recombinations. By tuning the energy levels of the two wells by an electric field *F*, the indirect exciton becomes the lowest-energy interband excitation.
2. As a matter of fact, the direct exciton peak energy experiences a small downward quadratic Stark shift which is equal to half of the product of the induced dipole by the field *F* [90]. On the other hand, the indirect exciton energy depends linearly on *F* with a slope that is proportional to the separation distance between the two well centers.
3. The electric field dependence of the exciton binding energy (E_B) is more than an order of magnitude weaker that that of the exciton peak energy. Binding energies of indirect excitons in the GaAs/AlGaAs CQW structure have been determined by exact solutions of the Schrödinger equation. It is possible to show that the calculated E_B is almost constant for *F* = 5 - 40 kV/cm. Therefore, the change of E_B with the field can be neglected for high fields [11,14].
4. Moreover, the applied electric field modifies the wavefunction confinement in each of the well. Instead of spreading in each of the wells, the carriers become

essentially localized by triangular wells. This reduces the electron-hole overlap integral, thus increasing significantly the radiative lifetime [17].

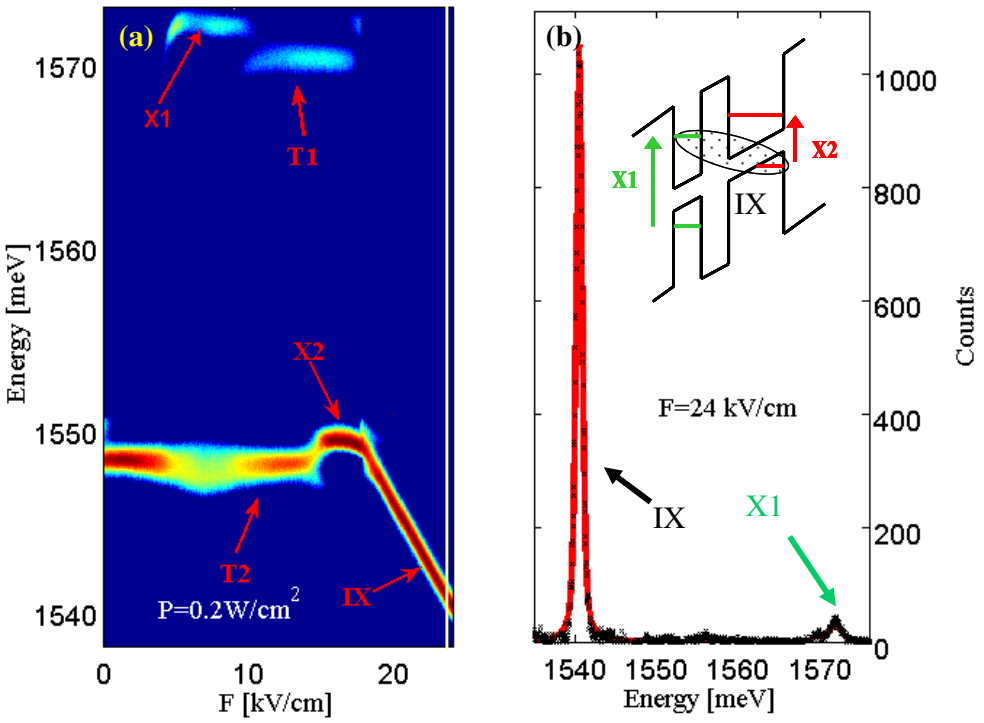

FIG. 6- **(a)** PL as function of applied electric field *F* in the asymmetric quantum well sample. The energies of the direct excitons of the narrow and wide wells are respectively E_{x1}=1572 meV and E_{x2}=1550 meV. The trions lines are respectively E_{t1}=1570 meV and E_{t2} =1548meV. The *IX* depends linearly on *F* with a slope of 1.35meV.kV^{-1}.cm .The excitation laser was a TiSaph laser tuned at 765nm with power intensity *P*=0.2 W/cm^2. The sample was immersed in superfluid helium at T=1.5K. **(b)** PL spectrum at *F*=24 kV/cm showing the indirect exciton line and the narrow well exciton line (X_1). **Inset** The energy band diagram of asymmetric coupled quantum wells under perpendicular applied electric field. X1 (in green) corresponds to the exciton in narrow well, X2 (in red) to the exciton in the wide well and IX (black ellipse) to the indirect exciton.

In Fig. 6a, we present the photoluminescence spectra (PL) as function of the applied electric field *F* and in Fig. 6b, we show the PL spectrum at a given electric field $F = 24$ kV/cm .

In the asymmetric system, the energies of the direct excitons of the narrow and wide wells are well separated which considerably facilitates the interpretation of the optical spectra.

The X_1 PL peak is assigned to a direct exciton transition involving an electron and a heavy-hole in the narrow well with peak energy $E_X^1 = E_g + E_e^1 + E_{hh}^1 - E_B^1$, where E_g is the GaAs bandgap, E_e^1 and E_{hh}^1 the first electron and heavy-hole subbands in the narrow well, and E_B^1 the binding energy of the exciton X_1.

The X_2 PL peak is assigned to a direct exciton transition involving an electron and a heavy-hole in the wide well with peak energy $E_X^2 = E_g + E_e^2 + E_{hh}^2 - E_B^2$, where E_g is the GaAs bandgap, E_e^2 and E_{hh}^2 the first electron and heavy-hole subbands in the wide well, and E_B^2 the binding energy of X_2.

As the electric field is changed, a line appears around 2 meV below the wide/narrow well exciton lines. Its evolution with magnetic field allows us to unambiguously identify it as the trion, a bound state of two electrons and a hole in the same well [91-93].

The indirect exciton energy depends linearly on F with a slope of $1.35\,\mathrm{meV.kV^{-1}cm}$. This linear dependence is due to the separation d=13.5 nm that separates the two well centers and can be directly obtained from equation (1.12) using first order perturbation theory:

$$\Delta E(F) = \left\langle \Psi(r_e, r_h) \middle| eF(z_e - z_h) \middle| \Psi(r_e, r_h) \right\rangle = eFd \qquad (2.1)$$

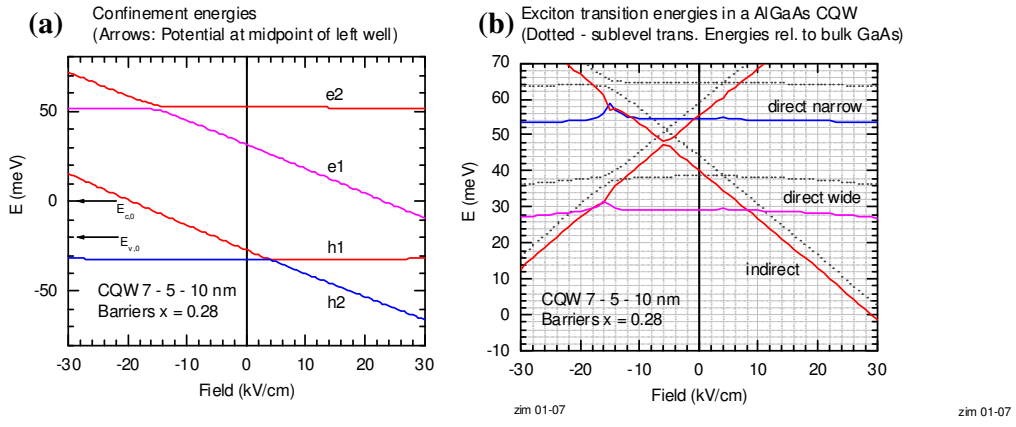

FIG. 7 – **(a)** Confinement energies of electrons and holes in the asymmetric system as function of applied electric field according to calculations performed by R. Zimmermann. **(b)** Exciton transition energies as function of applied electric field according to calculations performed by R. Zimmermann.

Figure 7 shows the results of more detailed calculations of the optical transition in this system performed by R. Zimmermann. The features that appear at ~-15 kV/cm for electrons and ~ 4 kV/cm for holes are related to sublevel degeneracy that the simulation was not able to treat properly.

In order to better understand the role of the electric field *F* on the radiative lifetime of excitons in our system, we performed a time-resolved measurement. The TiSaph excitation laser was modulated in amplitude by an acousto-optic modulator. It illuminated uniformly the whole sample. The luminescence was dispersed by a 75-cm spectrometer and detected using a cooled photomultiplier operated in photon counting mode. A temporal resolution of ~20 ns was achieved. In Fig. 8, the measured indirect exciton lifetime is plotted versus the applied electric field *F*. It is seen that an increase of the electric field of 6 kV/cm causes the measured recombination lifetime to increase by about an order of magnitude. The results of these measurements can be directly compared to those realized by Alexandrou *et al*. (Fig. 2c).

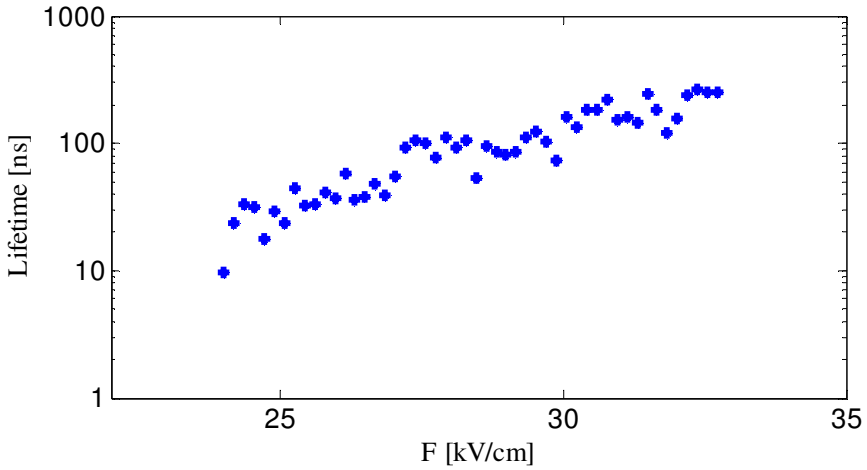

FIG. 8 – Lifetime of indirect excitons as function of applied electric field *F*. It is seen that the lifetime increases exponentially with *F*. An increase of 6 kV/cm causes an increase of the lifetime by around an order of magnitude.

2.1.3 Temperature of indirect excitons

The measurement of the exciton temperature is crucial in the road towards Bose-Einstein condensation. However, most works on indirect excitons have made the assumption that indirect excitons reach the lattice temperature due to their long lifetime but have no direct measure of their temperature.

Recently, Voros *et al.* [94-95] proposed a method based on the diffusion of indirect excitons in an in-plane harmonic trap. If the exciton density is low enough, such that interactions between the excitons can be ignored and particle statistics are in the classical limit, the spatial density profile of the excitons in equilibrium is given by the Boltzmann occupation factor

$$n(r) \propto \exp\left(-\frac{\alpha r^2}{2k_B T}\right) \equiv \exp\left(-\frac{r^2}{2\vartheta^2}\right) \tag{2.2}$$

where α is the spring constant of the trapping potential, ϑ the size of the cloud and T the temperature of the excitons. Therefore, the measure of the expansion of the exciton cloud in the trap gives directly an estimate of the temperature.

We measured the temperature of the exciton gas by using two different techniques.

In the first technique, the sample was illuminated by a Ti:Sapphire laser, which was focused on a $\sim 15\,\mu m$ diameter spot. A set-up of motorized lenses collected the PL from different points of the sample.

The PL intensity of an exciton system is due to cold excitons, which have a center of mass momentum smaller than the photon momentum. Higher momentum excitons need to slow down before they can recombine through photon emission. The PL intensity I_{PL} is defined by $I_{PL} = \frac{n_{lc}}{\tau_X^0}$ where n_{lc} is the density of the radiative excitons (those who reside within the light cone), and τ_X^0 is the exciton lifetime. One can define a temperature dependent lifetime $\tau_X(T)$ by $\frac{1}{\tau_X(T)} = \frac{n_{lc}}{n_X}\frac{1}{\tau_X^0}$ such that $I_{PL} = \frac{n_X}{\tau_X(T)}$. Thus, the exciton lifetime is reduced by the fraction of optically active excitons whose kinetic energy is below the light cone energy E_{lc} [96-98] and is given by:

$$\begin{aligned}\frac{1}{\tau_X(T)} &= \frac{1}{n\tau_X^0}\int_0^{E_{lc}} f(E)g_X(E)dE \\ &= \frac{1}{\tau_X^0} + \frac{2M}{\pi\hbar^2\tau_X^0 n_X}\left(\varsigma - E_{lc} + k_b T \ln\left[\exp\left[\frac{E-\varsigma}{k_B T}\right]-1\right]\right)\end{aligned} \tag{2.3}$$

where $\varsigma = k_B T \ln\left(1 - \exp\left(\frac{-\pi\hbar^2 n_X}{2Mk_b T}\right)\right)$ is the chemical potential of the exciton gas, *f(E)* is the occupation probability in Bose Einstein statistics and $g_X(E)$ is the density of states of excitons. It is easy to show that in the Maxwell Boltzmann limit, the exciton lifetime can be written as:

$$\frac{1}{\tau_X(T)} = \frac{1}{\tau_X^0}\left(1 - \exp\left(\frac{-E_{lc}}{k_B T}\right)\right) \qquad (2.4)$$

In Sec.2.2.3, we will show that the exciton peak energy gives us directly access to the local density of indirect excitons. Hence, by measuring the PL intensity at each location and assuming that far from the excitation spot the temperature of the indirect excitons is equal to that of the lattice, it is possible to estimate the profile of the exciton temperature.

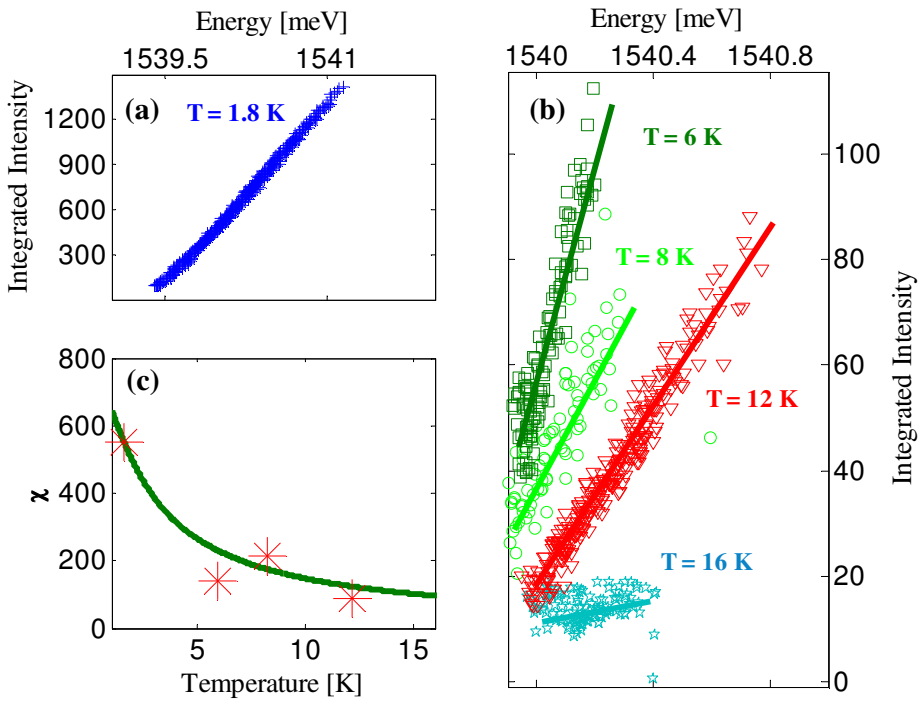

FIG. 9 – **(a)** PL intensity of indirect exciton as function of PL peak energy far from the excitation spot and at *T*=1.8 K. **(b)** PL intensity of indirect exciton as function of PL peak energy far from the excitation spot and at T= 6 K (dark green), 8 K (bright green) 12 K (red) and 16 K (turquoise). **(c)** Slope χ of graphs (a) and (b) as function of lattice temperature. The fit to experimental data (green line) gives $E_{lc} = 2.31\,\mathrm{K}$.

Figures 8a-b show the PL intensity I_{PL} as function of the indirect exciton peak energy (i.e. exciton density) at different lattice temperatures T. The PL intensity of indirect excitons is taken far from the excitation spot, such that their density is low enough to assume Maxwell Boltzmann statistics and their temperature is equal to the temperature of the lattice. As mentioned before, the indirect exciton peak energy shift is proportional to the local density (See Sec. 2.2.3) and therefore the slopes χ of Fig. 8a-b are inversely proportional to the indirect exciton lifetime. In Fig. 8c, we show the dependence of χ with temperature and it is possible to fit the experimental data to equation (2.3) with $E_{lc} = 2.31\,\mathrm{K}$.

The second technique for measuring the local temperature is based on the fact that the wide well direct excitons (X_2) and indirect excitons (IX) are in thermodynamic equilibrium. Assuming non degenerate and non interacting gases of X_2 and IX, we can write:

$$n_X = n_{IX} \exp\left(\frac{-\Delta E}{k_B T}\right) \tag{2.5}$$

where ΔE is the energy difference between the two states. Typically, this difference is of the order of 50 K and therefore at low temperature, most of the electron-hole pairs should form indirect excitons. However, we showed in Sec 2.1.2 that indirect exciton lifetime is very long and therefore the ratio of the PL intensities is larger than one might naively expect. The ratio η between the PL intensities of these two excitons is given by

$$\eta = \frac{I_{PL}^{IX}}{I_{PL}^{IX} + I_{PL}^{X}} \equiv \frac{1}{1 + \Gamma \exp\left[\frac{-\Delta E}{k_B T}\right]} \tag{2.6}$$

where Γ is the ratio of indirect and direct exciton lifetimes. To calibrate the curve and relate it to the temperature we performed a measurement of η as a function of lattice temperature with F=24 kV/cm in a broad spot and under very low excitation power, where one could safely assume that the excitons are at lattice temperature and ΔE constant (Fig. 10). It can be seen that the theoretical curves give a good fit to the data with $\Gamma = 300$ and $\Delta E = 6\,\mathrm{meV}$, in a good agreement with the expected values for these parameters.

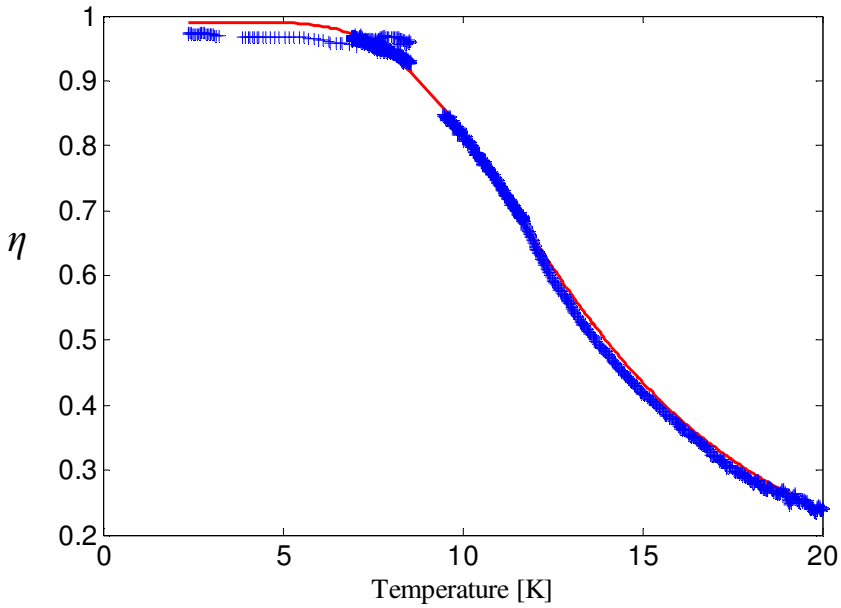

FIG. 10 – Ratio η between PL intensities of direct and indirect excitons as defined by (2.6) as function of lattice temperature under broad spot, very low excitation power and $F = 24$ kV/cm .

2.2 The Mott transition of Indirect Excitons in coupled Quantum Wells

In this chapter, we report the observation of the Mott transition of excitons in coupled quantum wells. The transition is manifested as an abrupt change in the conductivity and in the photoluminescence linewidth and peak energy at some critical power density and temperature. We measure the temperature dependence of the transition and determine the phase diagram of the system. We find that the transition is stimulated by the presence of direct excitons in one of the wells, and show that they serve as a catalyst of the transition. Indeed, we find that in the absence of these catalysts the phase transition is gradual.

2.2.1 Conductivity Measurements

The conductivity measurements seem to be the natural way to detect the Mott transition. As a matter of fact, this transition should be associated with a dramatic change of the conductance of the QW.

To be able to measure the in-plane conductance of the excitons we need to form ohmic contacts to the QWs. The usual procedure for making ohmic contacts to two dimensional electron or hole gas in GaAs QWs is to deposit a metallic layer on the sample surface and anneal it. This method has proven to be problematic for intrinsic QWs, in which the electrons and holes are photocreated: we found that the photo-excited carriers do not form good contact with the annealed region, and a non-linear I-V curve is observed [100]. We suspected that this is due to shadowing of the region close to the contacts by the metal layers. To solve this problem we developed an alternative technique in which the contacts are made to the *sides* of the QWs, and the annealed region is directly illuminated [101-102].

The mesa pattern consists of four rectangular contact region at the corner of a 100 μm wide square. In order to establish connections to the top gate and contacts, we used photodefinable polyimide (Probimide 7505). The polyimide is defined and cured before the self aligned contacts are made since it is not damaged by alloying of the contacts. To make the self aligned contacts, a layer of PMGI is applied to the sample. This photoresist is virtually insoluble in other photoresists and mostly sensible to UV exposure. The mesa is then defined by anisotropic $SiCl_4$ plasma etching up to a depth of 1.5 μm. The structure is wet etched to a depth 2000 Å below the quantum wells. A layer of image reversal photoresist (AZ 5214E) is patterned so as to expose the

regions where the contacts will be deposited. 300Å Ni followed by 1500Å of eutectic AuGe is evaporated on a rotating tilted stage. The photoresists are then removed with acetone and remover and the contacts are annealed at 475° C for 1 min in Rapid Thermal Processing (RTP). The metal connections are made with evaporated TiAu (250 Å Ti, 4000 Å Au) on rotating tilted stage.

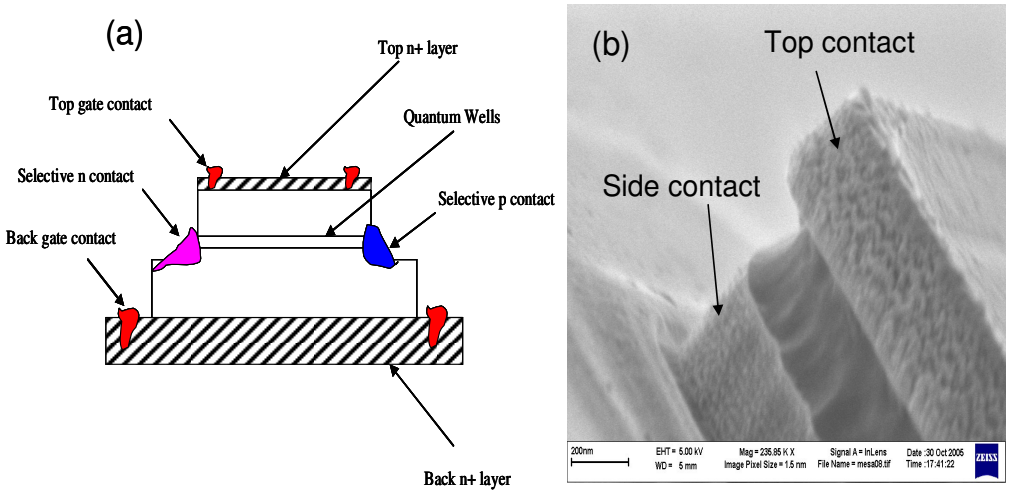

FIG. 11 - **(a)** Diagram of the MBE structure used in our work with evaporated and alloyed selective contacts. **(b)** SEM picture of a side contact.

Figure 11 shows the resulting system with its selective electrical contact to various layers of the structure allowing full control of the applied electric fields and detection of the current flowing both vertically and horizontally. Indeed, this method has proven to yield linear low resistance Ohmic contacts.

The conductance measurement is performed by applying a small ac voltage (10mV) to the side contacts, and using a lock-in amplifier to measure the photo-current. Figure 12a shows the in-plane conductance as a function of the illumination power density, P, at two vertical electric fields, F. It is seen that above a critical value of P ~ 0.5W/cm^2 there is a sharp change of the conductance: Approximately one order of magnitude conductance change in a power range of ΔP~50 mW/cm^2. This transition separates two different regimes: in the first region the resistance is of the order of 10 MΩ/□ whereas in the second region, the resistance is reduced to 0.5 MΩ/□. We note that the vertical electric field slightly shifts the transition point: the higher it is the lower the critical power density.

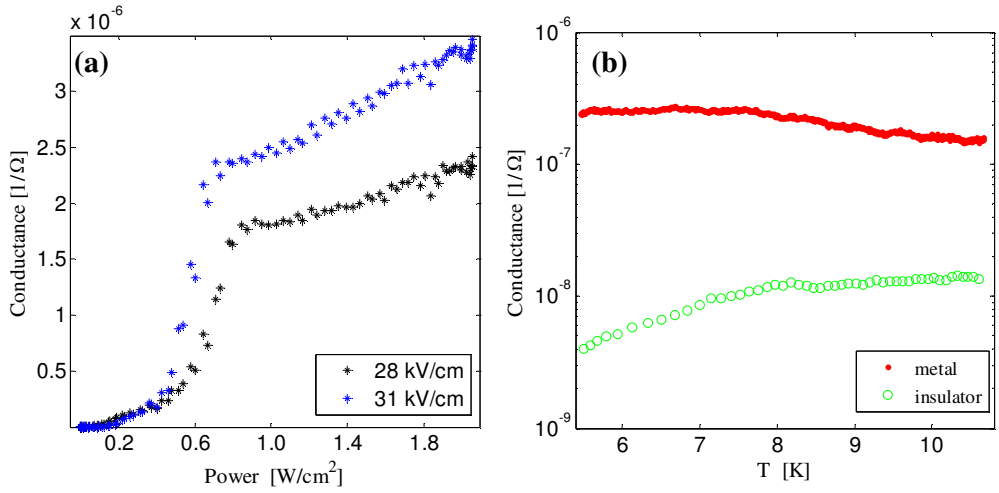

FIG. 12 - Conductivity measurements. (**a**) Measured conductance as function of laser excitation power at T=1.6K for two applied electric fields *F*=28 kV/cm and *F*=31 kV/cm. **(b)** Temperature dependence of the conductance in metallic and insulating phase for *F*=25.75 kV/cm.

We measured additionally the temperature dependence of the conductance at the two sides of the transition. In order to change the temperature adiabatically and to avoid bubbling and phase transitions of liquid helium, we put the sample in helium gas cooled down up to 4.2K; then we closed the needle valve and measured the conductance as function of time. In Fig. 12b we observed that below transition the conductance σ grows by a factor of 5 when the temperature is increased from 5 K to 10 K whereas above transition it decreases by a factor of 2 in the same range of temperatures. This result suggests that a metal insulator transition is taking place with $\partial\sigma/\partial T > 0$ in the insulating region and $\partial\sigma/\partial T < 0$ in the metallic region [103]. In that context it is plausible to examine the Mott scenario, in which a transition from an exciton gas to electron-hole plasma occurs above a critical density.

2.2.2 Diamagnetism of excitons

To get a deeper insight into the nature of the excited system, we measured the behavior of the PL energy as a function of magnetic field *B*, applied in Faraday configuration. It is well known that the exciton ground state energy increases quadratically with magnetic field, a phenomenon known as the exciton diamagnetic shift. As we shall see, this shift is proportional to the expectation value of the exciton radius squared. This is in contrast to uncorrelated electron-hole plasma, which exhibit

a linear dependence of the energy on *B*. Hence, by studying the magnetic field dependence of the PL energy we can determine the exciton radius, and study changes in it. Using this technique, we show that the transition is accompanied by a substantial change of exciton size, from being bound to unbound. Two regimes of diamagnetism are clearly observed, with a sharp boundary between a phase of bound excitons and a phase of unbound electron-hole plasma.

We would like first to review some well-known calculations [6] which will be useful for the understanding of our experimental results.

Within the framework of the effective mass approximation, the Hamiltonian H of an exciton in an heterostructure without magnetic field has been already given in (1.9). In presence of a magnetic field in Faraday configuration ($B \perp$ (x,y)), additional terms δH appears in the Hamiltonian:

$$\delta H = -\frac{e}{2}\left(\frac{1}{m_e^*} - \frac{1}{m_{hh/lh,\perp}^*}\right)\vec{B}\cdot\vec{\rho}\times\vec{p}_\perp - \frac{1}{m_e^* + m_{hh/lh,\perp}^*}\vec{P}_\perp \times \vec{B}\cdot\vec{\rho} + \frac{e^2\rho^2B^2}{8\mu^{hh/lh}} \qquad (2.7)$$

The first term of δH corresponds to the Zeeman term. It is linear in *B* and does not affect the 1s state which has a zero angular momentum. The second term arises from the quasi-electric field which an observer riding with the center of mass of the exciton would experience because of the magnetic field in the laboratory. It vanishes when the center of mass momentum of the exciton is equal to zero. The third term is the diamagnetic shift and increases quadratically with magnetic field.

In the case of photoluminescence, only the transitions between the electrons and heavy holes are observed. Therefore, the exciton ground state energy increases with magnetic field, $\Delta E(B) = \Lambda B^2 \langle \rho^2 \rangle$ where $\langle \rho^2 \rangle$ is the expectation value of the exciton radius squared and $\Lambda = \frac{e^2}{8\mu^{hh}}$. The value of μ^{hh} can be expressed in terms of the well-known Kohn Luttinger band parameters as shown in Eq. (1.2). We get $\mu^{hh} = 0.04\,\mathrm{m}_0$ and $\Lambda = 5.49 * 10^{-4}$ meV T^{-2}nm^{-2}. Hence, by studying the magnetic field dependence of the PL exciton energy we can determine the exciton radius, and study changes in it [104-105].

In the limit of unbound electrons and holes, the quadratic diamagnetism is expected to change into a linear dependence. It is well-known that the ground state energy of a quasi bi-dimensional electron (hole) gas subjected to a magnetic field in Faraday

configuration is shifted by $\hbar\omega_c/2$, where ω_c is the cyclotron frequency. In the case of an unbound electron-hole gas, the photoluminescence is therefore shifted by:

$$\Delta E(B) = \frac{e\hbar B}{2}\left(\frac{1}{m_e} + \frac{1}{m_{hh,\perp}}\right) \tag{2.8}$$

In GaAs quantum wells, this shift is approximately equal to ~ 0.9 meV/T.

To perform the PL measurements we prepared a larger area sample (1.5 mm^2), without the side contacts. Most of our studies focused on the asymmetric QW sample, where we could separately monitor the PL from each well. The mesa was illuminated by a laser spot which covered approximately a quarter of the area, and the PL was collected from a small spot of a few tens of microns in diameter. This ensures that the exciton density in the area from which we collect the PL is uniform.

Our first measurements concerned the diamagnetism of direct excitons in the 10-nm wide well. We found a diamagnetic shift $\Delta E(B) = 0.057B^2$ that corresponds to the expected radius $\langle\rho\rangle \approx 10\,\text{nm}$.

Fig. 13a shows a typical measurement of indirect exciton PL peak energy dependence on B with $E_L < E_{NW}$. A clear parabolic dispersion is seen throughout this density range, supporting the conclusion that the carriers are bound and form excitons. The in-plane radius of the indirect excitons can be readily extracted from this measurement and found to be ~20 nm.

It is also possible to estimate the binding energy of the direct and indirect excitons. We use a variational method introducing a trial wavefunction for indirect excitons of the following form: $\varphi(\rho) = N\exp\left[-\sqrt{\rho^2 + d^2}/\lambda\right]$ where d is the distance between the well centers, N the normalization factor and λ is the variational parameter.

The expectation values of the energy and the mean square radius are given by:

$$E = \langle\Psi|H|\Psi\rangle = \frac{e^2}{4\pi\varepsilon(2d+\lambda)} \tag{2.9}$$

$$\langle\rho^2\rangle = \langle\Psi|\rho^2|\Psi\rangle = \frac{\xi}{2}\frac{(3\lambda^2 + 4d^2 + 6\lambda d)}{2d+\lambda} \tag{2.10}$$

It is easy to see that for $d = 0$, the formulae give $\lambda = \frac{a_B}{2}$ and $\langle r^2 \rangle = \frac{3a_B^2}{8}$ corresponding to the usual pure 2D exciton formulae. We find that the binding energy of the indirect excitons in our structure is ~2.5 meV.

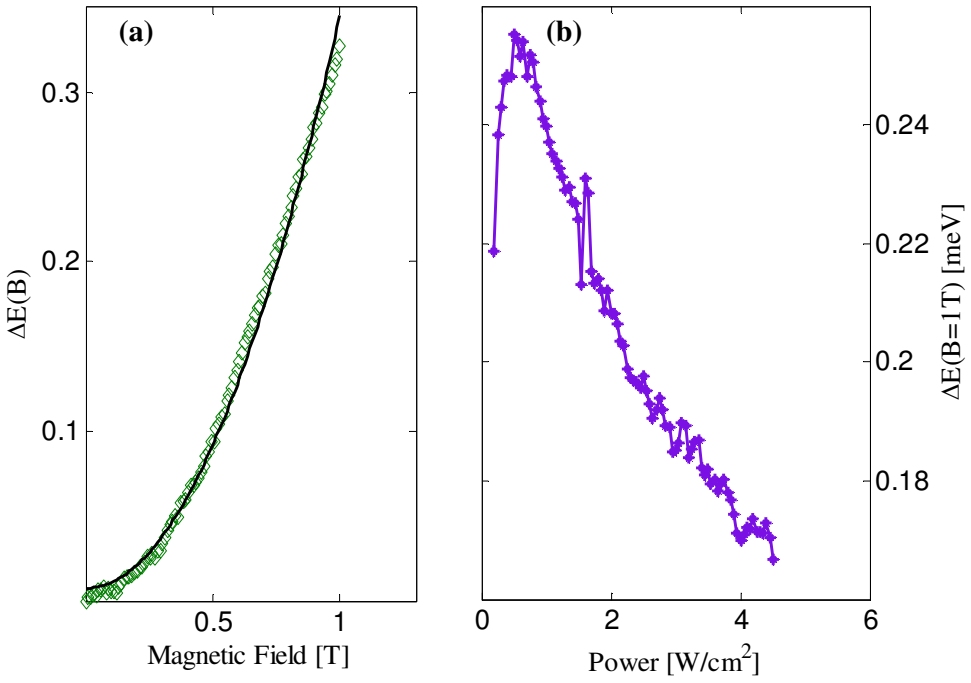

FIG. 13 – **(a)** Quadratic behavior of the peak energy as function of magnetic field applied in Faraday configuration. **(b)** The diamagnetic coefficient of the indirect exciton peak as function of power density with $E_L < E_{NW}$.

In Fig. 13b we observe that the diamagnetism decreases with increasing exciton density, indicating that the exciton radius becomes smaller at high density. This behavior is in complete contrast with the original Mott scenario, where the excitons are expected to be less bound as the density increases. Recently, Koch *et al.* predicted such a behavior using two different approaches: one based on calculation of dynamical density matrices, the second using a quantum Monte Carlo approach which allows to compute expectation values for a system of electrons and holes under their mutual Coulomb interaction in equilibrium [89] . In both cases, they observed a gradual decrease in the number of bound pairs while the remaining pairs are even stronger correlated than a single pair. This behavior is due to the possibility of the

electron–hole system to find spatial configurations where bound pairs are in segregated regions of space sufficiently far away from surrounding carriers such that possible screening effects are avoided.

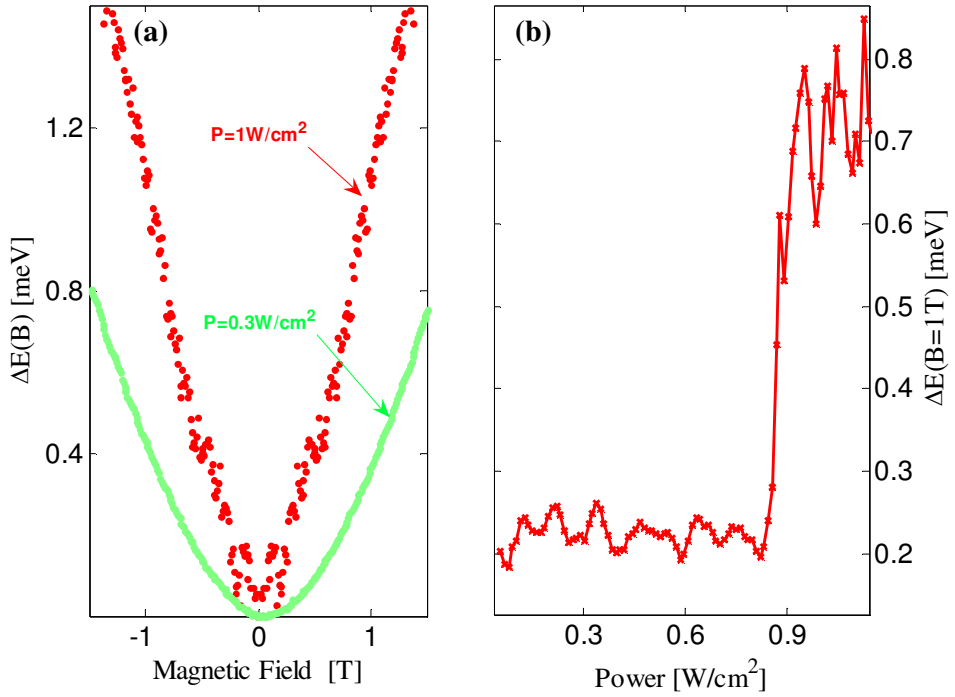

FIG. 14 – **(a)** Diamagnetism at two different power levels below and above the Mott transition with $E_L > E_{NW}$. **(c)** The diamagnetic coefficient as function of power density with $E_L > E_{NW}$.

Let us turn now into the second case of $E_L > E_{NW}$, where we get a mixture of direct and indirect excitons (See Sec. 2.1.1). Figure 14a shows the PL energy of indirect excitons as a function of magnetic field for $P = 0.3$ W/cm^2 and for $P = 1$ W/cm^2. One can clearly see how the quadratic behavior at low power densities turns into almost linear at high power. The in-plane radius of the indirect excitons at low power can be extracted from this measurement and is still found to be ~20 nm. Applying this analysis to the high power data yields a lower bound of ~ 50 nm for the exciton radius.

In Fig. 14b, we show the dependence of the diamagnetic shift $\Delta E(B = 1T)$ on power density and find an abrupt change at ~ 0.8 W/cm^2: two regimes of diamagnetism are

clearly observed, with a sharp boundary between a phase of bound excitons and a phase of unbound electron-hole plasma.

2.2.3 Density dependent blueshift

In the ideal electron-hole plasma regime, the separation of charges in the two wells creates an electric field, $F(n) = ne/\varepsilon$ which screens out the external electric field. The screening is proportional to the density of separated charges like in a capacitor and it shifts the recombination energy to higher values. This shift can be straightforwardly calculated using Eq. (2.1) as:

$$E_{elec} = ed \times (ne/\varepsilon) = ne^2 d/\varepsilon \qquad (2.11)$$

where n is the density of the uncorrelated electron-hole, d is the separation between the centers of the two wells and ε is the dielectric constant. In our system, the density of electron-hole plasma can thus be estimated by $n_{e-h} \approx 5.13 \times 10^9\,\mathrm{meV^{-1}\,cm^{-2}}$.

In the excitonic regime, the energy shift is primarily a many-body effect due to the exciton-exciton interactions. Indeed, indirect excitons are arranged as parallel dipoles, pointing to the same direction and, thus, exercise a repulsive force on each other.

The dipole-dipole interaction energy between two indirect excitons separated by a distance r can be written $U_{dd}(r) = (2\pi\varepsilon)^{-1}\left(e^2/r - e^2/\sqrt{r^2+d^2}\right)$ and therefore, the mean field interaction energy can be approximated by:

$$E_{meanfield} = \int U_{dd}(r) n d^2 r = E_{elec} \qquad (2.12)$$

As a result their average interaction energy should also increase with density, and be manifested by the same density dependent blueshift of the PL energy.

The density dependent blue shift for indirect excitons in the CQW structure has been calculated more precisely by Ben Tabou de-Leon *et al.* [106]. Following their calculations, the indirect exciton density should then be approximated in our asymmetric quantum well system by $n_{IX} \approx 7 \times 10^9\, meV^{-1} cm^{-2}$, which is higher but close to the density obtained from the capacitor formula of the ideal electron hole plasma.

However, this calculation does not take into account the correlations between electrons and holes. A theoretical description of exciton-exciton interactions in CQW was recently formulated by Zimmermann *et al.* [107-108]. They calculated the

exciton self energy in *a T-matrix approach* and found that a dramatic reduction of the interaction energy occurs at low temperatures. It was shown that the indirect exciton energy can be expressed as:

$$E_{\text{int}} = f(T) \times E_{elec} \tag{2.13}$$

The factor *f(T)* is small at cryogenic temperature, $f(2K) = 0.08$, and its origin is the strong depletion of the exciton gas around each exciton, which decreases the total energy of the system. Therefore, the indirect exciton density in our asymmetric quantum well system is given by $n_{IX} \approx 6.5 \times 10^{10} meV^{-1}cm^{-2}$.

An approximated expression for the correlation factor $f(T)$ can be obtained assuming that the probability of finding an exciton near a given exciton is $n \exp[-U_{dd} / k_B T] d^2 r$, one can writes the interaction term as:

$$\begin{aligned} E_{\text{int}} &= \int n U_{dd}(r) \exp\left[-\frac{U_{dd}(r)}{k_B T} \right] d^2 r \\ &= 2\pi n \int_0^\infty \left(1 - \frac{x}{\sqrt{x^2+1}} \right) \exp\left[\frac{-e^2}{2\pi\varepsilon d k_B T} \left(\frac{1}{x} - \frac{1}{\sqrt{x^2+1}} \right) \right] dx \end{aligned} \tag{2.14}$$

For $k_B T << \frac{e^2}{2\pi\varepsilon d}$, the main contribution to this integral comes from x>>1 and therefore we obtain:

$$f(T) \approx \Gamma(4/3) \times \sqrt[3]{\frac{\varepsilon d k_B T}{8e^2}} \tag{2.15}$$

This expression gives values (Fig. 15), which are very similar to those obtained more rigorously by Schindler and Zimmermann [108].

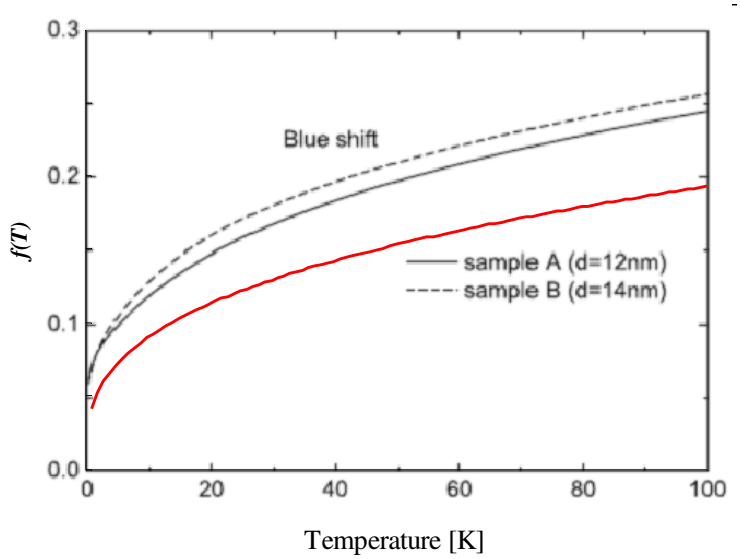

FIG. 15 - The correlation factor $f(T)$ as function of lattice temperature. The red line corresponds to the approximated expression given by Eq. (2.15) for our asymmetric coupled quantum well system (d=13.5 nm). The black lines correspond to the more detailed calculations of Schindler and Zimmermann [108] for two different samples. Sample A (solid line) is a CQW system formed by two 8-nm QWs separated by a 4-nm barrier. Sample B (dashed line) is a CQW system formed by two 10-nm QWs separated by a 4-nm barrier.

These considerations allow us to use the PL energy shift to determine the exciton density at the Mott transition. We find that the exciton density at the transition is $n \sim 2\times10^{10}\ \mathrm{cm}^{-2}$ at 1.8 K, implying that at the transition $na^2 \sim 0.3$, where $a \sim 40\ \mathrm{nm}$ is the indirect exciton diameter. To confirm this estimate we performed PL measurements at magnetic fields and determine the value of B, at which the lowest Landau level (LL) is full. At this magnetic field the PL from the second LL is diminished. This measurement can be conducted only at high carrier densities, well above the transition. We find that the carriers' density depends linearly on power, and we could therefore extrapolate the linear dependence to extract the density at the transition. This estimate agrees very well with that based on the blueshift.

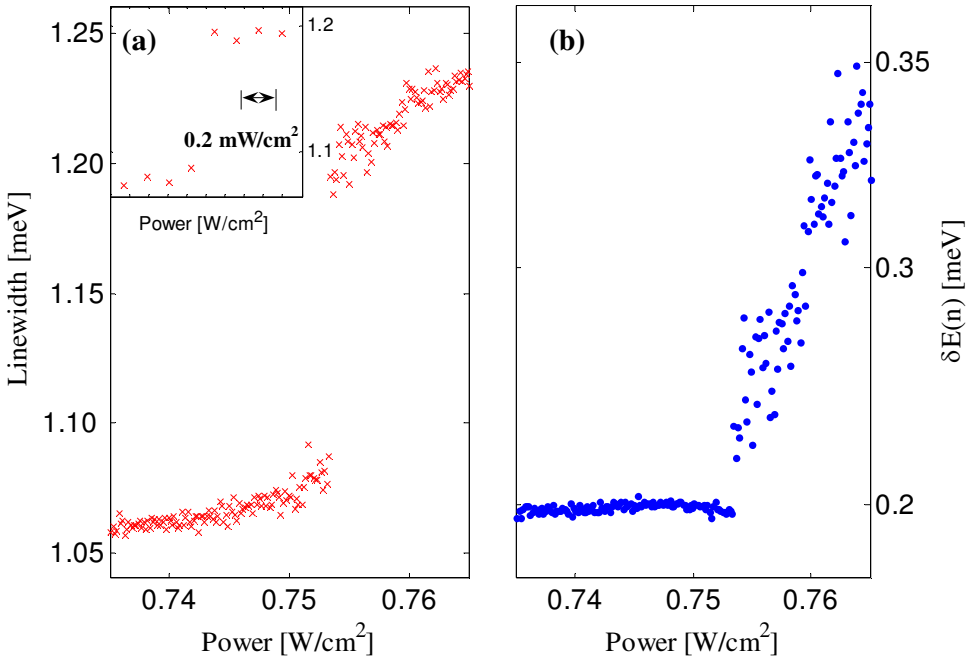

FIG. 16 - The PL properties as function of laser power at T=1.5 K and F=24 kV/cm. **(a)** Linewidth of IX line for $E_L > E_{NW}$ .The Mott transition is manifested by a jump of the linewidth by 25% at around 0.75W/cm^2. The inset demonstrates the abruptness of the transition, which occurs on less than 0.2mW/cm^2. **(b)** The PL energy shift δE for $E_L > E_{NW}$.

We find that the Mott transition is clearly manifested at the PL linewidth and energy at zero magnetic field. In fact, these studies allow us to better resolve the phase transition. This is demonstrated in Figure 16a which shows the dependence of the PL linewidth on P at 1.5 K. One can clearly distinguish two regimes, characterized by narrow and broad linewidth, with an *abrupt* transition between them. The inset shows a close-up view of the transition region, demonstrating the abruptness of the transition. We find that the transition becomes broader with increasing temperature, and extends to P~50 mW/cm^2 at 4.2K. It is interesting to note that the transition is accompanied by a modification of the lineshape from being predominantly Lorentzian to Gaussian. The behavior of the PL energy is somehow different (Figure 16b). Here we also find a transition, but it is manifested as a change in the slope of the energy versus P . The reason for that continuity is that one can not simply assume that the ionized electron-hole plasma remains at the gap energy, but should take into account interaction and band gap renormalization effects. This reminds the phenomenon

observed when increasing the density and monitoring the change of the PL spectrum from trion to 2DEG. There also we see the evolution of the 2DEG from the trion energy.

In the case of $E_L < E_{NW}$ -where only indirect excitons can be formed- we showed in Sec 2.2.2 that the carriers are bound in excitons even at very high power densities. In Figure 17a, we show the PL energy as a function of power density. We observe a relatively small blueshift of 0.6 meV as the power density is increased up to 4 W/cm^2. Using the calculations of Zimmermann, one can estimate the exciton density that corresponds to the observed blue-shift to be 6×10^{10} cm^{-2}. This density is comparable with the so-called Mott density $1/a_B$, where a_B is the exciton Bohr radius, yet no transition is observed. The presence of a high exciton density is also manifested in the PL spectrum: the linewidth increases by 50%, from 1 to 1.5 meV over this density range (Fig. 17b), while the integrated intensity grows precisely linearly with power.

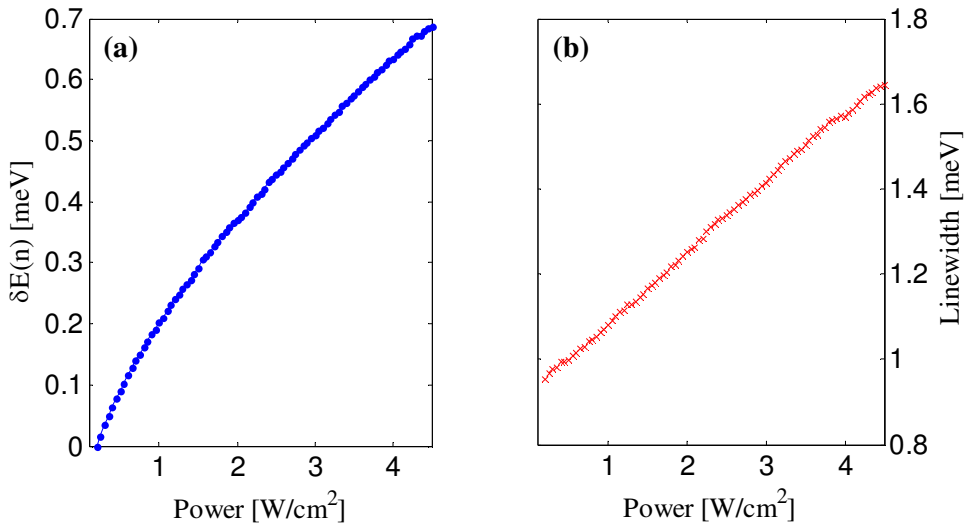

FIG. 17 – The PL properties as function of laser power at T=1.5 K and F=24 kV/cm for $E_L < E_{NW}$. **(a)** The PL energy shift δE of IX line **(b)** The linewidth of IX line.

2.2.4 Role of the excitation energy

To summarize our results thus far we find that all different measurements, i.e. electrical conductance, exciton diamagnetism, PL linewidth and PL energy show an

abrupt phase transition from exciton gas to electron-hole plasma at the same critical parameters. We note that this behavior is very different from that of direct exciton gas in a single QW, where a gradual transition is observed. A natural question to ask is what is the underlying mechanism that distinguishes this system and gives rise to the observed phase transition. As we shall show below, the abruptness of the transition is the result of a *catalytic process* due to the presence of direct excitons in the narrow well.

The key experiment in understanding the origin of the transition is measuring its dependence on the excitation laser energy, E_L. We find that the phase transition is not observed when E_L is chosen such that carriers are excited in the wide well only (Fig. 18b). In that case, the photo-excited electrons quickly tunnel in the direction of the electric field to the narrow-well and complete charge separation is achieved. The resulting system is simple and consists of electrons in the narrow well and holes in the wide well, which are bound to form indirect excitons. Indeed, no other luminescence line is observed (under sufficiently large electric field). This behavior is radically changed when we create carriers also in the narrow well, $E_L > E_{hh}^{NW}$, where E_{hh}^{NW} is the heavy hole exciton energy in the narrow well. The holes in the narrow well tunnel along the field direction into the wide well, but with a much longer tunneling time. As a consequence, some of the holes may bind with electrons in the narrow well and form a direct exciton. Indeed, at low excitation power we observe a weak excitonic line from the narrow-well. Hence, we have at low densities a mixed phase of *IX*+*X*. As the power increases and crosses the transition threshold the PL spectrum changes, and a new line appears 2.1 meV below the narrow well exciton (Fig. 18c). Its evolution with electric field allows us to unambiguously identify it as the narrow well trion, *T*, a bound state of two electrons and a hole in the same well [91-93].

The appearance of trion luminescence is not surprising: it is well known that this is the ground state of a system consisting of a majority of electrons and minority of holes. Hence, we are at the situation where the electrons in the narrow well have a choice, either to bind to a hole in the wide well and form an indirect exciton, or to bind to an exciton in the narrow well and form *T*. Since the indirect exciton binding energy is lower than that of the *T*, 2.5 vs. 2.1 meV, this is the ground state at low densities. Apparently, upon increasing the carrier's density, it becomes more favorable to form trions. The transition can be described by the reaction $IX + X \rightarrow T + h$. We note, however, that the trions are not stable and rapidly decay through the process

$T \rightarrow e + h\nu$. Since the rate of this decay process is much faster than the rate of trion formation, more and more indirect excitons dissociate and the concentration of free electrons and holes increases up to the Mott criterion. The presence of direct excitons serves as a catalyst of the reaction, and an abrupt transition from bound exciton to free electron-hole plasma occurs.

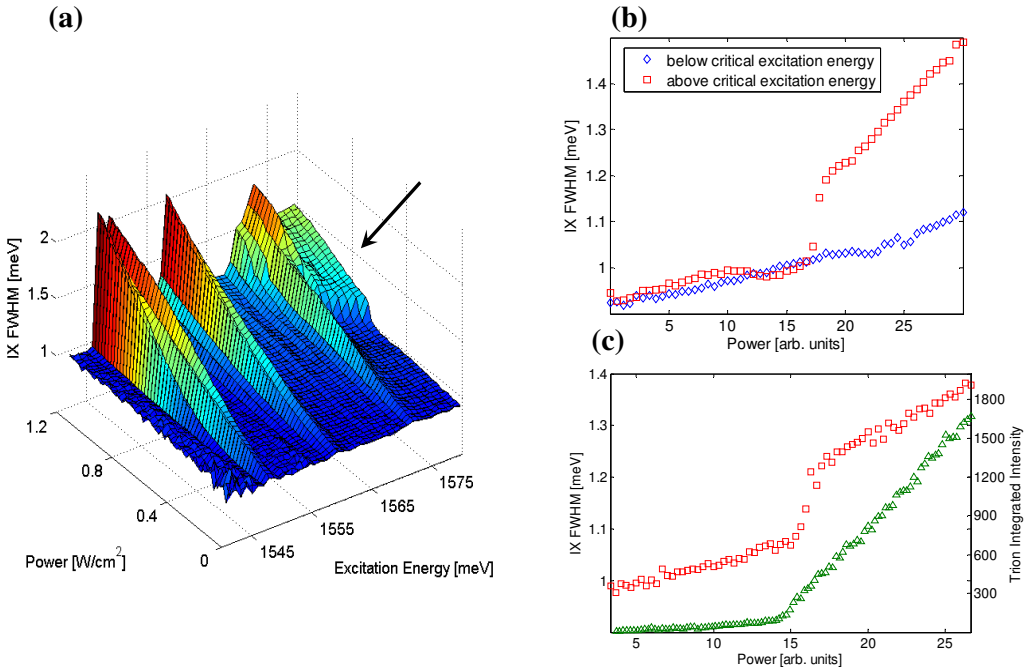

FIG. 18 - Direct excitons and trions near the transition. . **(a)** Indirect exciton linewidth as function of excitation laser energy and power for T=1.6K, and F=24kV/cm. The transition (marked by the arrow) only occurs when the excitation energy is above the narrow well exciton energy. **(b)** Indirect exciton linewidth as function of power intensity above and below critical excitation energy **(c)** Trion integrated intensity (green Δ) as function of power.

The measurement of the dependence of the PL linewidth on the excitation laser energy and power (Figure 18a) provides a supporting evidence for this scenario. It is seen that the abrupt transition (marked by the arrow) indeed occurs only at $E_L > E_{hh}^{NW}$. The three peaks which are seen correspond (from low to high energy) to the heavy and light hole excitons in wide well, E_{hh}^{WW} and E_{lh}^{WW} , and the heavy hole exciton in the narrow well, E_{hh}^{NW} . The fact that the PL width is broader at those energies stems from the fact that at these resonances the absorption is enhanced, and hence the photo-

created electron density is larger. We can see that the broadening of the indirect exciton PL width is gradual when $E_L < E_{hh}^{NW}$, and becomes abrupt only when $E_L > E_{hh}^{NW}$, namely when excitons in the narrow-well can be created.

2.2.5 Temperature dependence of the Mott transition

To establish the fact that this is indeed a thermodynamic phase transition we measured the temperature dependence of the transition. Figure 19b shows the evolution of the PL width with temperature at fixed *P*. We find that at low temperatures (*T*=1.6K) the linewidth is broad (1.8 meV), characteristic of unbound electron-hole plasma. As the temperature is increased the width decreases rapidly and levels at 1.3 meV above 3K. As the temperature increases further we observe an opposite transition above 6 K – the PL linewidth turns from excitonic to electron-hole plasma. The same re-entrance behavior is observed when examining the blue shift of the PL energy. This behavior implies that at this power density an excitonic phase exists only in a limited range, 3 K < *T* < 6 K, and it turns into electron-hole plasma below and above this range.

The phase diagram in the *P*-*T* plane is depicted in Figure. 19a (the dashed line describes the measurement of Figure. 19b). One can see that the excitonic phase indeed exists only in a limited area in this parameter space.

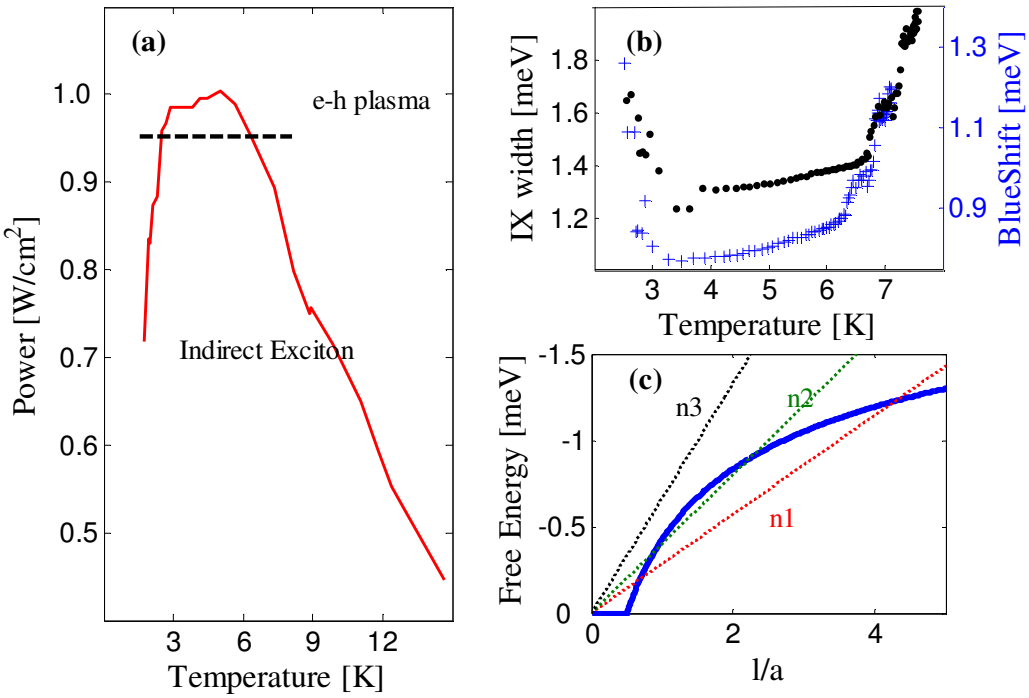

FIG. 19 - Temperature dependence of the transition. **(a)** The power-temperature phase diagram showing the indirect exciton and electron-hole plasma regions for F=24 kV/cm. The dashed line corresponds to the parameters of b. **(b)** Linewidth and blueshift as function of temperature for P ~ 0.95 W/cm^2 and F=24 kV/cm. **(c)** The free energy of screened excitons (solid line) and electron-hole plasma (dashed lines) for different total pair densities as function of the screening length l.

As a conclusion, we wish to suggest a qualitative explanation for the unique shape of the temperature phase diagram. Let us consider two states of the system: a bound exciton gas and a pure free electron-hole plasma.

First, we assume that the screening of the excitonic interaction is due to the free electrons and holes, and that the screening length l can be estimated within the Thomas Fermi approximation by:

$$l = \frac{2\varepsilon k_B T}{e^2 n_e} \qquad (2.16)$$

where n_e is the free electron density.

Second, we consider the exciton and electron-hole gases as non degenerate and non interacting gases. Below the Mott transition, the free energy of a system composed of N electron-hole pairs can be written as:

$$F_X = (N-n)\left[k_B T + E_B\left(l/a_B\right) - Ts_X\right] + n\left[2k_B T - Ts_{e-h}\right] \qquad (2.17)$$

where E_B is the screened binding energy of the excitons, n the number of unbound electrons and holes, s_X and s_{e-h} the entropic terms for excitons and unbound electron-hole plasma respectively.

Above the Mott transition, the free energy of the system composed of N unbound electrons and holes can be written simply as:

$$F_{e-h} = N\left[2k_B T - Ts_{eh}\right] \qquad (2.18)$$

The ground state of the system can therefore be determined by comparing F_X and F_{e-h}, and the transition line is determined by solving $F_X - F_{e-h} = 0$ which can be simplify to:

$$E_B = T\left[k_B + s_X - s_{e-h}\right] \qquad (2.19)$$

A graphical solution of Eq. (2.19) is provided in Figure 14c for several densities of free electron-hole pairs n_1, n_2 and n_3. The blue line describes some generic dependence of E_B on $l \propto T/n$. It is seen that this equation has two solutions for a wide range of values, and no solution beyond a certain value, as indeed observed experimentally. While this model provides a qualitative understanding of the transition it is very simplified: it considers the exciton screening within a simple approximation and neglects changes in the exciton distribution which should modify the system's entropy. Furthermore, it neglects interaction effects and band gap renormalization in the electron-hole plasma.

2.3 Excitonic and Ambipolar Diffusion in Coupled Quantum Wells

In the previous part of this work, we focused mainly our investigation on local measurements of the exciton system. Indeed, we found drastic changes of diamagnetism and photoluminescence properties at the phase transition from exciton gas to electron-hole plasma. In this chapter, we will show that the Mott transition of excitons in coupled quantum wells is also manifested by a macroscopic effect: a sharp change in the diffusion properties of the electron-hole pairs.

In the recent years, several groups performed detailed studies of exciton flow by means of optical spectroscopy. As a matter of fact, the long lifetime of indirect excitons and their strong repulsive interaction give rise to a large diffusion length, conveniently accessed using optical techniques [25-27]. Recently, the observation of two PL intensity rings around the excitation spot reported by Butov *et al*. raised controversy. While it was shown that the external ring is due to the creation of excess free carriers in the quantum well [28-29], the origin of the inner ring was attributed to the cooling down of the excitons as they diffuse away from the hotter excitation spot. It was claimed that excitons exhibit bosonic properties which modify dramatically their diffusion coefficient when the density is sufficiently high [30-31]. We will show in the following chapter that the formation of this ring is not the result of such bosonic features but characterizes the diffusion of unbound electrons and holes as they diffuse away from the hotter excitation spot and cool down.

2.3.1 Exciton Diffusion

In order to study the exciton diffusion, we built an experimental setup capable of performing a spatial imaging of the photoluminescence in a magnetic field. The sample was mounted in a window cryostat equipped with a split coil. The TiSaph excitation laser was focused tightly on a region of ~15µm diameter. A set-up of motorized lenses collected the spectra from different points of the sample. The resolution of the imaging system was ~3µm. We performed these measurements at various excitation powers and lattice temperatures.

The laser energy was tuned to be 1.56 eV, which is slightly above the wide QW gap but below the narrow well gap. We applied an electric field of 24kV/cm perpendicular to the QWs, such that the electron level in the wide well is higher than that of the narrow well. Under these conditions direct excitons are formed in the wide well only,

and electrons tunnel efficiently into the narrow well to form indirect excitons (See Sec. 2.1.1).

Figure 20 summarizes our experimental results at low excitation power. In Fig. 20a we show the PL intensity profile of the indirect excitons (solid line). For comparison we also show the PL profile of the direct excitons, when the electric field is set to zero. It can be clearly seen that the indirect excitons diffuse to large distances of ~10μm, while the direct excitons diffusion length is at least an order of magnitude smaller. This large diffusion length does not reflect a larger diffusion coefficient of the indirect excitons but is rather a straightforward result of their different lifetimes: the diffusion length is given by $\sqrt{D\tau}$, and the direct and indirect exciton life times differ by ~ 2 orders of magnitude. Hence, to a good approximation the direct exciton intensity profile can serve as a measure of the spot size.

To get an insight into the nature of the system under this excitation power, we measured the behavior of the PL energy as function of magnetic field B applied in a Faraday configuration at a few spatial points along the diffusion profile. As was shown in Sec 2.2.2, this measurement can distinguish between exciton gas and free electron-hole plasma: the exciton ground state energy should increase quadratically with magnetic field while uncorrelated electron-hole plasma should exhibit a linear dependence of the energy on B. In Fig. 20b we show the PL energy as a function of magnetic field at the center of the excitation spot, where the density is highest. One can clearly observe a quadratic behavior, which characterizes a bound exciton. This quadratic behavior is observed at any measured location along the PL profile, supporting the conclusion that the diffusing carriers at this excitation power are bound excitons.

Figure 20c shows the PL energy shift as function of the distance from the center of the excitation point. This energy shift $\delta E(n)$ is primarly a many-body effect due to the exciton-exciton interactions (Sec. 2.2.3). The value of $\delta E(n)$ at the center is ~1 meV, corresponding to a total density $n_{IX} \sim 5\times10^{10}\ cm^{-2}$. The fact that the blueshift decreases with distance is a manifestation of the decrease of the steady state density with distance due to recombination and expansion of the exciton gas. We note, however, that the blueshift curve does not follow exactly the PL intensity curve. This is due to the slight heating of the lattice at the center of the excitation spot. We recall that the PL intensity of an exciton system is due to cold excitons, whose center of

mass momentum is smaller than the photon momentum. Excitons with center of mass energy higher than the light cone energy, E_{lc}, need to slow down before they can recombine through photon emission. The PL intensity is related to the total density by $I_{PL} = \frac{n}{\tau}\left(1 - \exp\left(\frac{-E_{lc}}{k_B T}\right)\right)$, and hence, the luminescence from hotter regions is suppressed (Sec 2.1.3).

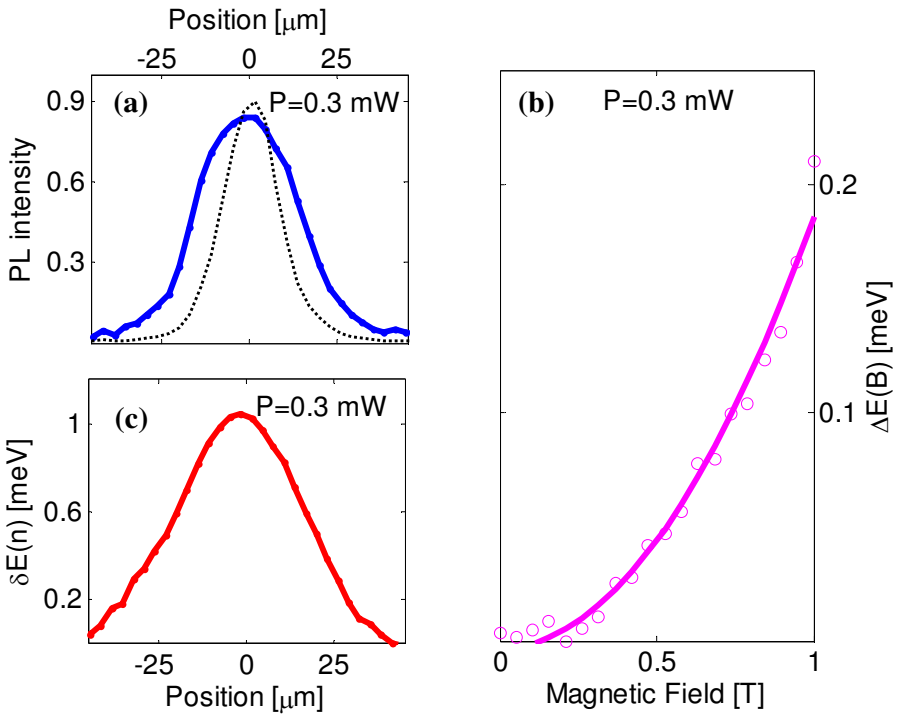

FIG. 20 - **(a)** The PL intensity profile of indirect excitons at F=24 kV/cm, T=1.8K (solid). The dashed line is the direct exciton profile at F=0, which gives the spot size. **(b)** The PL energy shift of indirect excitons as function of magnetic field. The solid line is a fit to a quadratic diamagnetic behavior. **(c)** The PL energy shift of indirect excitons as function of position.

2.3.2 Ring Formation

The behavior mentioned above changes drastically at high excitation powers. While the spatially resolved PL of the direct excitons is not modified compared to previous experiments, the PL intensity of indirect recombinations forms a non-trivial pattern and we observe the formation of a PL intensity ring around the excitation spot. The typical radius of this ring is ~20 μm as shown in Figure 21a.

As mentioned before, the observation of a PL ring around the excitation spot was reported by several groups in the last years. The origin of this ring was attributed to the cooling down of the excitons as they diffuse away from the hotter excitation spot. A detailed hydrodynamic model was proposed to describe this diffusion, and predicted a high degeneracy of the exciton gas [30-31]. This was perceived as a step towards Bose Einstein condensation, and an optical trap which is based on this effect was demonstrated [32-33].

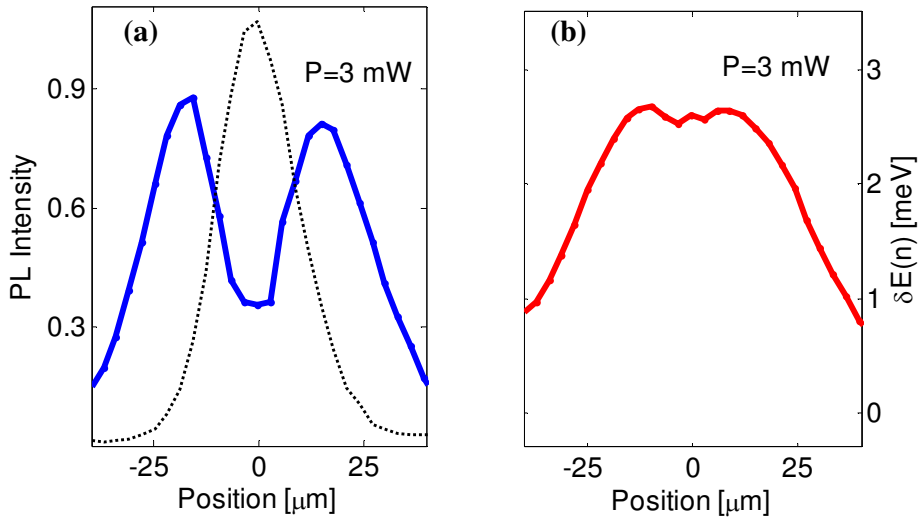

FIG. 21 – **(a)** The PL intensity profile of indirect recombinations (solid) and direct exciton (dashed). **(b)** The PL energy shift of indirect recombinations as function of position. **(c)** The PL energy as function of applied magnetic at 3 points at distances of 18, 36 and 54 microns from excitation spot center (respectively blue crosses , red points and green crosses). **(d)** The PL linewidth as function of laser power at 18 microns from the spot center.

We shall show below that the interpretation of this ring formation in terms of excitonic diffusion is incorrect. As a matter of fact, we found that the ring pattern appears when performing the experiment at relatively high lattice temperatures, as high as 15K. At these temperature ranges, the excitons are expected to ionize and certainly to behave as Maxwell-Boltzmann rather than Bose-Einstein gas.

Rather, the formation of the PL ring is due to ambipolar diffusion of unbound electrons and holes. In that sense, the ring formation is a vivid demonstration of the Mott transition, from excitons to unbound electron-hole plasma.

Figure 16b describes the PL energy shift, $\delta E(n)$, as a function of distance from the spot center. It is seen that the energy profile is flat at the center, $\delta E \approx 2.5\,\mathrm{meV}$, and then decreases monotonously. If we assume that the diffusing pairs are bound excitons and use Eq. (2.13) to determine their density, we are led to conclude that this blueshift corresponds to a very high exciton density, of ~1.5×10^{11} cm^{-2}, well above the Mott transition in this system. We note that large PL blueshifts were also observed in Ref. [32], and interpreted in terms of excitons. However, the expression used to determine the density omitted the *f(T)* correlation factor, and therefore underestimated the corresponding exciton density by an order of magnitude.

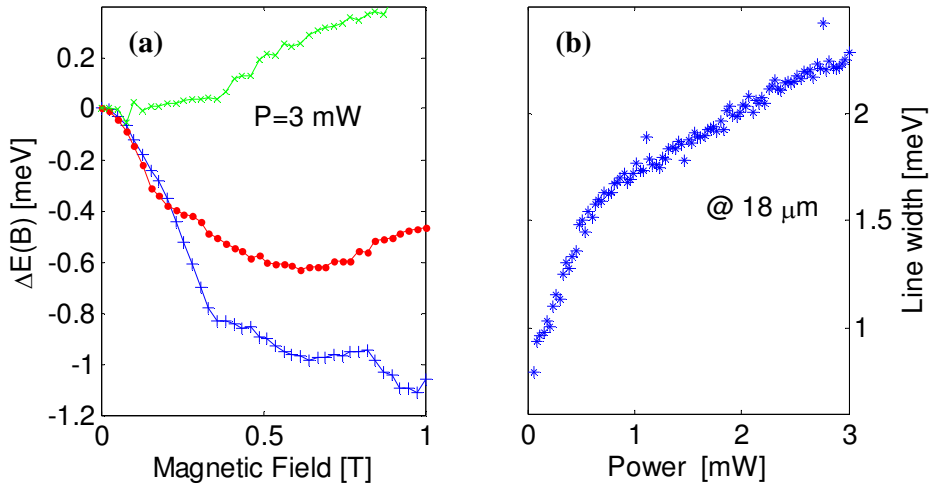

FIG. 22 - . **(a)** The PL energy as function of applied magnetic at 3 points at distances of 18, 36 and 54 microns from excitation spot center (respectively blue crosses , red points and green crosses). **(b)** The PL linewidth as function of laser power at 18 microns from the spot center.

Once again, the key experiment to distinguish between electron-hole plasma and exciton phase is measuring the diamagnetic shift. Thus, we spatially resolve and measure the PL peak energy as function of the applied magnetic field *B* (Fig. 22a). We found that far from the excitation spot, the behavior is quadratic, indicating that excitons are formed (Sec 2.2.2). This behavior is completely changed as we get closer to the center of the spot: rather than an increase of the PL energy, we observe a red shift as function of the magnetic field. The shape of this redshift is position dependent as shown on Figure 22a. Its origin is the Lorentz force acting on charged particles,

which suppresses their diffusion and reduces their steady state density far from the spot center. This reduction in density is manifested as a decrease of the PL energy relative to the energy at B=0 (Sec. 2.2.3).

Furthermore, we performed several PL measurements as function of the excitation power. We set the excitation wavelength such that direct excitons can be formed in both wells. In that situation, it was shown previously that the Mott transition is characterized by an abrupt change of the PL linewidth. Indeed, we observed that the appearance of the PL ring is accompanied with a change of the behavior of the PL width, indicating a change in the nature of the system (Fig. 22b). At the transition, two distinct lines appear in the spatially integrated PL spectrum separated by around 2 meV.

These results clearly show that at high powers the diffusing particles are unbound electrons and holes.

3.3.3 Exciton and ambipolar diffusion

The precedent observations clearly show that the formation of the PL ring is due to electron-hole plasma rather than exciton diffusion. While it is not surprising that excitons undergo a Mott transition at high power density, a major question remains open: why are the exciton and electron-hole plasma diffusion so different? As we shall show below the diffusion of unbound electron and holes is much faster than that of bound pairs, by approximately an order of magnitude at cryogenic temperatures, and the ring formation is due to "the giant ambipolar diffusion" [109-110] of electron-hole plasma in coupled quantum wells.

The indirect exciton diffusion is described by the following equation diffusion-drift equation:

$$\frac{\partial n_{IX}}{\partial t} = -\vec{\nabla}\cdot\vec{j}_{IX} + S \qquad (2.20)$$

$$= D_X \nabla^2 n_{IX} + \vec{\nabla}\cdot(\mu_X n_{IX}\vec{\nabla}E_{\text{int}}) + S \qquad (2.21)$$

where D_X, n_{IX} and μ_X are the diffusion coefficient, density and mobility of the excitons, respectively, E_{int} is the exciton-exciton interaction energy and S corresponds to the rate of generation/annihilation of excitons. The first term in Eq. (2.21) describes a regular diffusion process due to a density gradient, while the second term is the one which is due to the interaction. To compare the two terms we use the

Einstein relation, $\mu_X = D_X / k_B T$, and Eq. (2.13) to write the diffusion current as follows :

$$\vec{j}_{IX} = -D_X (1 + E_{\text{int}} / k_B T) \vec{\nabla} n_{IX} \qquad (2.22)$$

It is seen that the interaction term is dominant when $E_{\text{int}} >> k_B T$, implying that interaction energies of a few tenths of meV are sufficient to overcome the regular diffusion at cryogenic temperatures.

In the case of the diffusion of unbound electron and hole plasma, it is possible to write the two different diffusion-drift equations for electrons and holes as :

$$\frac{\partial n_{e,h}}{\partial t} = D_{e,h} \nabla^2 n_{e,h} \pm e\vec{\nabla} \cdot (n_{e,h} \mu_{e,h} \vec{\nabla} \phi_{e,h}) + S \qquad (2.23)$$

where $\phi_{e,h}$ is the electrical potential in the electron and hole layer given by:

$$\phi_e = \frac{e}{4\pi\varepsilon} \int \left[\frac{n_h(\vec{r})}{\sqrt{r^2 + d^2}} - \frac{n_e(\vec{r})}{|\vec{r}|} \right] d^2 \vec{r} \qquad (2.24)$$

$$\phi_h = \frac{e}{4\pi\varepsilon} \int \left[\frac{n_h(\vec{r})}{|\vec{r}|} - \frac{n_e(\vec{r})}{\sqrt{r^2 + d^2}} \right] d^2 \vec{r} \qquad (2.25)$$

An important property of this system is its local charge neutrality: The separation of different sign carriers costs electrostatic energy and the system minimizes it by keeping equal local densities of electrons and holes, e.g $n_e(x, y) = n_h(x, y) \equiv n$. In coupled quantum wells, this is equivalent to assuming that the characteristic screening length is much smaller than the diffusion length. Under this assumption one can combine the equations (2.23) and write the following diffusion equation:

$$\frac{\partial n}{\partial t} = D_A \nabla^2 n + \frac{e}{2} \vec{\nabla} \cdot \left(n \mu_A \vec{\nabla} \left(\phi_e - \phi_h \right) \right) + \text{S} \qquad (2.26)$$

where $D_A = \dfrac{2 D_e D_h}{D_e + D_h}$ is the ambipolar diffusion coefficient and μ_A is the ambipolar mobility. It is possible to explicitly calculate the electrostatic term when d is much smaller than the space scale in the plane of the QWs:

$$e\left(\phi_e(r)-\phi_h(r)\right)=\frac{e^2}{\varepsilon}\int_0^{\infty}n(x)\left[\frac{x}{\sqrt{x^2+d^2}}-1\right]dx$$
$$\sim\frac{-e^2}{\varepsilon}n(r)d\equiv -E_{elec} \qquad (2.27)$$

Writing Eq. (2.26) in the form of (2.20) and using Einstein relation, we get the ambipolar diffusion current

$$\vec{j}_A=-D_A\left(1+E_{elec}/2k_BT\right)\vec{\nabla}n \qquad (2.28)$$

where E_{elec} is the electrostatic energy density of the electron hole system.

Comparing the two cases, of exciton and ambipolar diffusion, we reach a surprising result, that the diffusion of unbound electron and holes is much faster than that of bound pairs, by a factor $f(T)$, which amounts to approximately an order of magnitude at cryogenic temperatures.

3.3.4 Numerical solutions

We solved numerically Eqs. (2.21) and (2.23) by finite element simulations in 2D assuming a radial symmetry of the laser profile and Dirichlet conditions at the edge of the computational domain. In order to match the model with our experimental data, we fitted the model by minimizing the mean square deviation of the data from the computed curves.

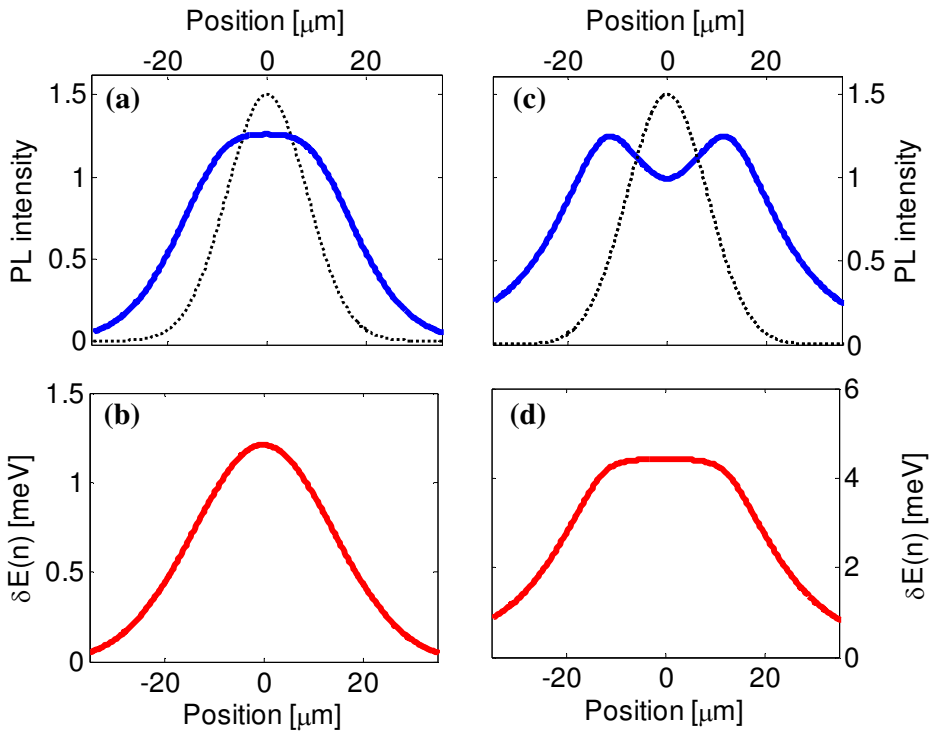

FIG. 23 – Numerical solutions of the diffusion equation for the excitons ((a) & (b)) and for the electron-hole plasma ((c) & (d))

We adopted the following approach: once we selected the free parameters for the fit and their broad ranges, we performed a grid evaluation of squared deviations on the parameter space, in order to locate approximately the set of parameter values giving the absolute minimum. At this point, we used standard nonlinear fit routine to refine the estimation. This approach was required as the strong nonlinear dependencies of the model create several local optimization minima within the plausible parameter range, and a simple gradient-based minimum search might fail.

The resulting temperature agrees well with our independent measurements using the PL intensities of the direct and indirect excitons, Eq. (2.6). We find that we could reproduce the bell shape of the excitonic diffusion, the ring pattern of the PL intensity and the plateau in the density profile in the case of ambipolar diffusion.

3. Conclusions

3.1 Nature of the Mott transition

The Mott transition of indirect excitons in coupled quantum wells is found to be a gradual transition accompanied with the decrease of exciton radius with density of electron-hole pairs. This behavior is in complete contrast with the original Mott scenario, where the excitons are expected to be less bound as the density increases but in good agreement with S. Koch's recent predictions. Contrary to other metal-insulator transitions where the electrons move but the ions are arranged in lattice, the exciton binding energy depends weakly on density because the excitons can move without restrictions. Therefore, the system finds spatial configurations, where bound pairs are in segregated regions of space, sufficiently far away from surrounding carriers and such that possible screening effects are avoided.

In a mixture of indirect excitons and direct excitons, the transition becomes extremely abrupt. It is manifested as a sharp change in the conductivity and in the photoluminescence properties of the system. It is accompanied by a substantial change of exciton size, from ~20nm below the critical density to more than 50 nm above. We proposed, in this work, a qualitative model to explain the underlying mechanism that distinguishes the two systems, but a more detailed analysis is required to fully understand the role of trions at the Mott transition.

Clearly, more experiments and theory on this interesting system are needed. For example, we observed fluctuations of the electron-hole plasma recombination energy above the Mott transition (Fig. 14a and Fig. 16b). The origin of such fluctuations could be a kind of hysteresis with regions of bistability in which the number of free carriers depends on the history of the system.

3.2 Exciton-exciton interactions

Indirect excitons are arranged as parallel dipoles, pointing to the same direction. The interaction between these dipoles causes a shift of the photoluminescence energy and generates a strong force, which drives the excitons away from each other. However, exciton correlations reduce this interaction energy by a factor $f(T)$ due to a strong depletion of the exciton gas around each exciton.

In Fig. 24 we show the blueshift of the PL energy as a function of intensity in a broad spot (250 μm diameter) experiment. The PL was collected from a small area of a few tens of microns in diameter, ensuring that the exciton density in the area where we collected the PL is constant. The change in slope at the Mott transition is clearly visible, and is due to the different density dependence of the PL energy, $\delta E(n)$, in the two sides of the transition. Using the expressions for E_{int} and E_{elec}, we determine the correlation factor $f(T)$ by the ratio between the two slopes. We find that $f(T=1.5K)=0.05$, and that its temperature dependence is very close to the prediction of Zimmermann *et al.* [108].

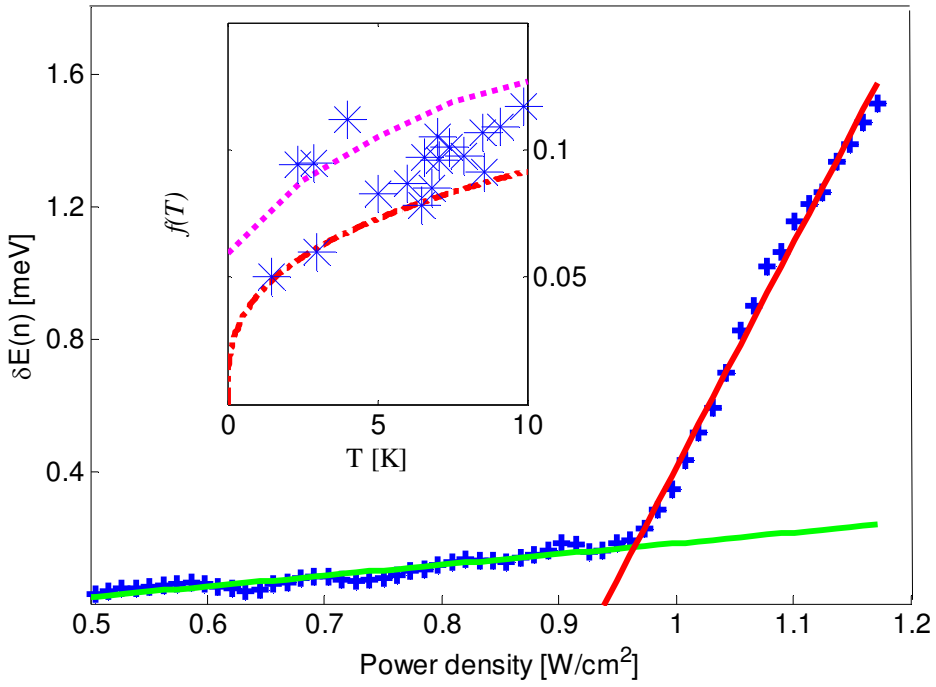

FIG. 24 - The blueshift of the PL energy as a function of intensity in a broad spot (250 μm diameter) experiment around the Mott transition. The solid lines are linear fits in the exciton and electron-hole regimes. The ratio of their slopes yields $f(T=1.5K)=0.05$. (**inset**) The measured values of the correlation factor f as function of temperature. The lines are the theoretical calculation of Ref.[108] (dashed) and Eq. (2.15) (dot-dashed).

The correlations between excitons have major consequences in terms of diffusion of photogenerated carriers below and above the Mott transition. The transition is strongly manifested as a very large increase of the diffusion coefficient, by approximately an order of magnitude, as the system changes from bound excitons to

unbound electrons and holes. This change in diffusion coefficient together with local heating at the illumination spot gives rise to a ring pattern of the PL intensity. Our work disproves some previous claims that the ring formation is due to a change of the excitonic diffusion near the BEC transition and can be used to form an excitonic trap. Rather, we show that when the PL ring is observed the system consists of unbound electrons and holes, way above the Mott transition.

We reach the surprising result that the diffusion of unbound electron and holes is much faster than that of bound pairs, by a factor $f(T)$, which amounts to approximately an order of magnitude at cryogenic temperatures.

The giant ambipolar diffusion of unbound electrons and holes in coupled quantum wells offers very interesting perspectives of research. Using our demonstrated technique for establishing different p and n selective contacts on the same sample (Sec. 2.2.1), it should be possible to observe strong drag phenomena in coupled quantum wells at relatively high temperatures.

3.3 Towards a BEC of excitons?

We measured the temperature dependence of the transition and determined the phase diagram of the system. Interestingly, we observe a re-entrance behavior: for a given power density, an excitonic phase exists only in a limited range and it turns into electron-hole plasma below and above this range. To understand this behavior, we constructed a phenomenological model which takes into account the changes in entropy of the system. While this model provides a qualitative understanding of the transition, it is oversimplified and neglects changes in the exciton distribution which should modify the system's entropy. This required a more detailed analysis which was beyond the scope of this work.

The Mott transition hinders the formation of an indirect exciton dense gas and it seems difficult to reach BEC conditions in this framework. Therefore, lower temperatures should be reached: the Kosterlitz-Thouless critical temperature varies linearly with the concentration of excitons, while - at least theoretically - the Mott transition is not expected at sufficiently low density, when the Coulomb interaction is not screened.

Over the past thirty years, there have been numerous claims of observations of Bose Einstein condensation or superfluidity of excitons. They were followed by much

debate and many retractations. Indeed, a reliable way to detect the condensate is needed. For instance, theoretical studies have shown that the condensate should reveal itself in a very narrow line surrounded by wings and therefore luminescence line shape measurements may be interpreted as an indication of Bose statistics of excitons. Another prediction is that a spatially varying potential should lead the gas to condense at its center with the appearance of a sharp peak. However, both approaches are essentially measurements of the energy distribution while separating the condensate from low excited states is difficult.

Therefore, a qualitative experiment that would produce a signature of the exciton condensate is desirable. Hopefully, a Bose condensate is characterized not just by a macroscopic number of particles in the ground state, but also and mainly by its coherent nature. The coherence of the condensate should be manifested for example by an interference pattern of the luminescence from two parts of the condensate. In that context, the measurement of second order correlation function of the exciton luminescence was recently suggested by B. Laikhtmann [66]. This measurement should allow to measure directly the order parameter in the Bose condensed exciton gas. Another possible direction was recently proposed by Lilly *et al* [111]. The idea is to measure the drag and counterflow transport properties of an indirect exciton supercurrent in the separately contacted layers. Especially, for the counterflow setup the steady state current should be carried by the condensate only. Therefore no voltage drop in both layers is expected. Moreover, the noise of the current fluctuations in such a system can provide a signature of the condensate state.

4. References

[1] G. Bastard, *Wave mechanics applied to semiconductor heterostructures* (Editions de Physique, Les Ulis, France, 1988).

[2] M. A. Herman, H. Sitter, *Molecular Beam Epitaxy* (Springer-Verlag, Heidelberg, 1989).

[3] Landolt-Bornstein, *Numerical Data and Functional Relationships in Science and Technology,* Springer-Verlag, **III-22b,** 218-223 (1989).

[4] Z. Ikonic, V. Milanovic and D. Tjapkin, *Valence subband structure of [100]-grown, [110]-grown and [111]-grown GaAs/AlGaAs quantum wells and the accuracy of the axial approximation,* Phys. Rev. B, **46**, 4285 (1992).

[5] G.H. Wannier, *The structure of electronic excitation levels in insulating crystals*, Phys. Rev., **52**, 191 (1937).

[6] R.S. Knox, *The theory of Excitons* (Academic Press, New York, 1963).

[7] E.I. Rashba and M.D. Sturge, *Excitons* (North Holland Library, Netherlands, 1987).

[8] B. Zaslow and M.E. Zandler, *Two dimensional Analog to the Hydrogen Atom*, Am. J. Phys., **35**, 1118 (1967).

[9] R.C. Miller, D.A. Kleinman, W.T. Tsang and A.C. Gossard, *Observation of the excited level of excitons in GaAs quantum wells,* Phys. Rev. B, **24**, 1134 (1981).

[10] R.L. Greene, K.K. Bajaj and D.E Phelps, *Energy levels of Wannier excitons in GaAs/AlGaAs quantum well structures,* Phys. Rev. B, **29**, 1807 (1984).

[11] Y. Takahashi, *The effect of electric field on the excitonic states in coupled quantum well structures,* J. Appl. Phys., **76**, 2299 (1994).

[12] I. Linnerud and K.A. Chao, *Exciton binding energies and oscillator strengths in a symmetric AlGaAs/GaAs double quantum well,* Phys. Rev. B, **49**, 8487 (1994).

[13] S. Ben Tabou de Leon and B. Laikhtman, *Exciton wave function, binding energy and lifetime in InAs/GaSb coupled quantum wells,* Phys. Rev. B, **61**, 2874 (2000).

[14] M.H. Szymanska and P.B. Littlewood, *Excitonic binding in coupled quantum wells,* Phys. Rev. B, **67**, 193305 (2003).

[15] S. Charbonneau, M.L.W. Thewalt, E.S. Koteles, B. Elman, *Transformation of spatially direct to spatially indirect excitons in double quantum wells*, Phys. Rev. B, **38**, 6287 (1988).

[16] J.E. Golub *et al*, *Long-lived spatially indirect excitons in coupled GaAs/AlGaAs Quantum Wells,* Phys. Rev. B, **41**, 8564 (1990).

[17] A. Alexandrou *et al*, *Electric field effects on exciton lifetimes in symmetrical coupled GaAs/AlGaAs double quantum wells,* Phys Rev. B, **42**, 9225 (1990).

[18] T.C. Damen *et al*., *Dynamics of exciton formation and relaxation in GaAs quantum wells,* Phys. Rev. B, **42**, 7434 (1990).

[19] R. Strobel, R. Eccleston, J. Kuhl and K. Kohler, *Measurement of the exciton formation time and the electron tunnelling and hole tunnelling times in a double quantum well structure",* Phys. Rev. B, **43**, 12564 (1991).

[20] D. Robart *et al*., *Dynamical Equilibrium between excitons and free carriers in quantum wells,* Solid State Commun., **95**, 287 (1995).

[21] H.X. Jiang *et al*., *Dynamics of exciton transfer between the bound and continuum states in GaAs/AlGaAs multiple quantum wells,* Phys. Rev. B, **41**,12949 (1990).

[22] C. Piermarocchi *et al*., *Exciton formation rates in GaAs/AlGaAs quantum wells,* Phys. Rev. B, **55**, 1333 (1997).

[23] S. Siggelkow *et al*., *Exciton formation and stability in semiconductor heterostructure,* Phys. Rev. B, **69**, 73104 (2004).

[24] J. Szczytko *et al*., *Determination of the Exciton Formation in Quantum Wells from Time Resolved Interband Luminescence,* Phys. Rev. Lett., **93**, 137401 (2004).

[25] L.V. Butov, A.C. Gossard and D.S. Chemla, *Macroscopically ordered state in an exciton system*, Nature, **418**, 751 (2002).

[26] D. Snoke *et al*., *Long range transport in excitonic dark states in coupled quantum wells*, Nature, **418**, 754 (2002).

[27] Z. Voros *et al*., *Long Distance Diffusion of Excitons in Double Quantum Well Structures,* Phys. Rev. Lett., **94**, 226401 (2005).

[28] I.V. Kukushkin *et al*., *Reduction of the electron density in GaAs-AlGaAs single heterojunctions by continuous photoexcitation,* Phys. Rev. B, **40**, 4179 (1989).

[29] R. Rapaport *et al.*, *Charge Separation of Dense Two Dimensional Electron-Hole Gases: Mechanism for Exciton Ring Pattern Formation,* Phys. Rev. Lett., **92**, 117405 (2004).

[30] A. L. Ivanov, *Quantum diffusion of dipole oriented indirect excitons in coupled quantum wells*, EuroPhys. Lett., **59**. 586-591 (2002).

[31] A. L. Ivanov *et al.*, *Origin of the inner ring in photoluminescence patterns of quantum well excitons,* EuroPhys. Lett., **73**, 920-926 (2006).

[32] A.T. Hammack, *Trapping of Cold Excitons in Quantum Well Structures with Laser Light,* Phys. Rev. Lett., **96**, 227402 (2006).

[33] A.T. Hammack *et al.*, *Kinetics of indirect excitons in an optically induced trap in GaAs quantum wells,* Phys. Rev. B, **76,** 193308 (2007).

[34] A. Griffin, D.W. Snoke, S. Stringari, *Bose Einstein Condensation* (University Press, Cambridge, 1995).

[35] L.D. Landau and E.M. Lifshits, *Statistical Physics, Part I*, **62** (Pergamon Press, Oxford, 1993).

[36] M.H. Anderson, J. R. Ensher, M.R. Matthews, C.E. Wieman and E.A. Cornell, *Observation of bose-einstein condensation in a dilute atomic vapor*, Science, **269**, 198 (1995).

[38] K.B. Davis *et al*., *Bose-einstein condensation in a gas of sodium atoms* , Phys. Rev. Lett., **75**, 3969 (1995).

[39] J.M. Blatt, W. Brandt and K. W. Boer, *Bose Einstein condensation of excitons*, Phys. Rev. **126**, 1691 (1962).

[40] L.V. Keldysh, A.N. Kozlov, *Collective properties of excitons in semiconductors*, Soviet Phys. JETP, **27**, 521 (1968).

[41] C. Comte and P. Nozieres, *Exciton Bose condensation – the ground-state of an electron-hole gas*, J. Phys-Paris **43,** 1069-1083 (1982).

[42] L.L. Chase, N.Peyghambarian, G. Grinberg, A. Mysyrowicz , *Evidence for Bose Einstein Condensation in Biexcitons in CuCl,* Phys. Rev. Lett., **42**, 1231 (1979).

[43] N.Peyghambarian, L.L. Chase and A. Mysyrowicz, *Bose Einstein statistical properties and condensation of excitonic molecules in CuCl,* Phys. Rev. B, **27**, 2325 (1983).

[44] M. Hasuo, N. Nagasawa, T. Itoh and A. Mysyrowicz, *Progress in the Bose Einstein Condensation of biexcitons in CuCl,* Phys. Rev. Lett., **70**, 1303 (1993).

[45] D. W. Snoke, J.P. Wolfe and A. Mysyrowicz, *Quantum Saturation of a Bose gas : excitons in Cu_2O,* Phys. Rev. Lett. **59**, 827 (1987).

[46] J.J. Lin and J.P. Wolfe, *Bose Einstein condensation of paraexcitons in stressed Cu_2O,* Phys. Rev. Lett., **71**, 1222 (1993).

[47] A. Mysyrowicz, E. Benson and E. Fortin, *Directed Beam of Excitons Produced by Stimulated Scattering,* Phys. Rev. Lett., **77**, 896 (1996).

[48] D.W. Snoke and V. Negoita, *Pushing the Auger limit: Kinetics of excitons in traps in Cu_2O,* Phys. Rev. B, **61**, 2904 (2000).

[49] S. Denev and D.W. Snoke, *Stress dependence of exciton relaxation processes in Cu_2O*, Phys. Rev. B, **65**, 085211 (2002).

[50] S. Pau *et al.*, *Observation of a laserlike transition in a microcavity exciton-polariton system,* Phys. Rev. A, **54**, R1789 (1996).

[51] H.Deng *et al*., *Condensation of Semiconductor Microcavity Exciton-Polaritons,* Science, **298**,199-202 (2002).

[52] M. Richard *et al*., *Spontaneous coherent phase transition of polaritons in CdTe microcavities,* Phys. Rev. Lett., **94**, 187401 (2005).

[53] J. Kasprzak *et al*., *Bose Einstein Condensation of Exciton polaritons*, Nature, **443**, 409-414 (2006).

[54] H. Deng *et al*., *Quantum Degenerate Exciton-Polaritons in thermal Equilibrium,* Phys. Rev. Lett., **97**,146402 (2006).

[55] T. Fukuzawa, E.E. Mendez, and J.M. Hong, *Phase transition of an exciton system in GaAs coupled quantum wells*, Phys. Rev. Lett., **64**, 3066 (1990).

[56] J.A. Kash *et al*., *Fermi Dirac distribution of excitons in coupled quantum wells,* Phys. Rev. Lett., **66**, 2247 (1991).

[57] X. Zhu, P.B. Littlewood, M.S. Hybertsen and T.M. Rice, *Exciton condensate in semiconductor quantum-well structures*, Phys. Rev. Lett., **74**, 1633 (1995).

[58] Y.E. Lozovik and O.L. Berman, *Phase transitions in a system of spatially separated electrons and holes,* JETP, **84**, 1027 (1997).

[59] V.B. Timofeev *et al*., *Phase diagram of a two dimensional liquid in GaAs/AlGaAs biased double quantum wells,* Phys. Rev. B, **61**, 8420 (2000).

[60] L. V. Butov *et al*, *Stimulated scattering of indirect excitons in coupled quantum wells: Signature of a degenerate bose-gas of excitons,* Phys. Rev. Lett., **86**, 5608 (2001).

[61] V. Negoita, D.W. Snoke and K. Eberl, *Harmonic potential traps for indirect excitons in coupled quantum wells,* Phys. Rev. B, **60**, 2661 (1999).

[62] L.V. Butov *et al*., *Towards bose-einstein condensation of excitons in potential traps*, Nature, **417**, 47 (2002).

[63] A. Gartner *et al*, *Micro patterned electrostatic traps for indirect excitons in coupled GaAs quantum wells,* Phys. Rev. B, **76**, 085304 (2007).

[64] C.W. Lai, J.Zoch, A.C. Gossard and D.S. Chemla, *Phase diagram of degenerate exciton systems*, Science, **303,** 503 (2004).

[65] J.P. Eisenstein and A.H. MacDonald, *Bose Einstein condensation of excitons in*

bilayer electron systems, Nature, **432**, 691 (2004).

[66] B. Laikhtman, *Coherence of the exciton condensate luminescence,* Europhys. Lett., **43**, 53-58 (1998).

[67] M. Combescot and C. Tanguy, *New criteria for bosonic behavior of excitons*, Europhys. Lett., **55,** 390 (2001).

[68] D.W Snoke, *When should we say we have observed Bose condensation of excitons ?,* Phys. Stat. Sol. (b), **238**, 389-396 (2003).

[69] V. Bagnato, D. E. Pritchard and D.Kleppner, *Bose Einstein condensation in an external potential,* Phys Rev A, **35**, 4354 (1987).

[70] V. Bagnato and D. Kleppner, *Bose Einstein condensation in low-dimensional traps*, Phys. Rev. A, **44**, 7439 (1991).

[71] V. N. Popov, *On the theory of the superfluidity of two- and one- dimensional bose systems*, Theor. Math. Phys. **11**, 565-573 (1973).

[72] N.F. Mott, *Metal Insulator Transitions* (Taylor and Francis, London, 1990).

[73] T.M. Rice *et al*., *The Electron Hole Liquid in Semiconductors* (Solid State Phys., **32**, 1977).

[74] D.W. Snoke, *Predicting the ionization threshold for carriers in excited semiconductors,* private communications (2007).

[75] G.A. Thomas and T.M. Rice, *Trions, molecules and excitons above the Mott density in Ge,* Solid State Commun., **23**, 359 (1976).

[76] J. Shah, M. Combescot and A.H. Dayem, *Investigation of Exciton Plasma Mott transition in Si*, Phys Rev. Lett., **38**, 1497 (1977).

[77] G.A. Thomas, J.B. Mock and M. Capizzi, *Mott distortion of the electron-hole fluid phase diagram,* Phys. Rev. B, **18**,4250 (1978).

[78] A. Forchel *et al*., *Systematics of electron-hole liquid condensation from studies of silicon with varying uniaxial stress,* Phys. Rev. B, **25**, 2730 (1982).

[79] L.J. Schowalter, F.M. Steranka, M.B. Salamon and J.P. Wolfe, *Evidence for separate Mott and liquid-gas transitions in photo-excited, strained germanium,* Phys. Rev. B, **29**, 2970 (1984).

[80] L.M. Smith and J.P.Wolfe, *Second Condensed Phase of Electron Hole Plasma in Si*, Phys. Rev. Lett., **57**, 2314 (1986).

[81] A.H. Simon, S.J. Kirch and J.P. Wolfe, *Excitonic phase diagram in unstressed Ge,* Phys. Rev B, **46**, 10098 (1992).

[82] A. Amo *et al*., *Photoluminescence dynamics in GaAs along an optically induced Mott transition,* J. Appl. Phys. **101**, 081717 (2007).

[83] L. Kappei *et al*., *Direct Observation of the Mott transition in an Optically Excited Semiconductor Quantum Well,* Phys. Rev. Lett., **94**, 147403 (2005).

[84] G.B. Norris and K.K. Bajaj, *Exciton-Plasma Mott transition in Si,* Phys. Rev. B, **26**, 6706 (1982).

[85] R. Zimmermann, *Non linear optics and Mott transition in semiconductors,* Phys. Stat. Sol (b), **146**. 371 (1988).

[86] D.W. Snoke and J.D. Crawford, *Hysteresis in the Mott transition between plasma and insulating gas,* Phys. Rev. E, **52**, 5796 (1995).

[87] S. Ben Tabou de Leon, B. Laikhtman, *Mott transition, biexciton crossover and spin ordering in the exciton gas in quantum wells,* Phys. Rev. B, **67**, 235315 (2003).

[88] V.V Nikolaev and M.E. Portnoi, *Theory of excitonic Mott transition in double quantum wells,* Phys. Stat. Sol (c), **1**, 1357 (2004).

[89] S.W. Koch *et al*., *Exciton Ionization in semiconductors,* Phys. Stat. Sol. (b), 238, 404 (2003).

[90] L. Vina *et al*., *Stark shifts in GaAs/AlGaAs quantum wells studied by photoluminescence spectroscopy,* J. Phys.C **20**, 2803 (1987).

[91] G. Finkelstein, H. Shtrikman and I. Bar-Joseph, *Optical Spectroscopy of a Two-Dimensional Electron Gas near the Metal Insulator Transition,* Phys. Rev. Lett.,74, 976 (1995).

[92] S.I. Gubarev *et al*., *Screening of excitonic states by low-density 2D charge carriers in GaAs/AlGaAs quantum wells,* JETP Lett., **72**, 324 (2000).

[93] I. Bar-Joseph, *Trions in GaAs quantum wells,* Semiconductor Science and Technology, **20**, 6R29 (2005).

[94] Z. Voros, D.W. Snoke, L. Pfeiffer and K. West, *Trapping Excitons in a Two-dimensional In-Plane Harmonic Potential: Experimental Evidence for Equilibration of Indirect Excitons,* Phys. Rev. Lett., **97,** 016803 (2006).

[95] Z. Voros *et al*, *Considerations on equilibration of two-dimensional excitons in coupled quantum wells,* J. Phys.: Condens. Matter, **19**, 295216 (2007).

[96] J. Feldmann *et al*, *Linewidth dependence of radiative exciton lifetimes in quantum wells,* Phys. Rev. Lett., **59**, 2337 (1987).

[97] B. Deveaud *et al.*, *Enhanced Radiative Recombination of Free Excitons in GaAs Quantum Wells,* Phys. Rev. Lett., **67**, 2355 (1991).

[98] L.C. Andreani, F. Tassone and F. Bassani, *Radiative lifetime of free excitons in quantum wells,* Solid State Comm., **77,** 641-645 (1991).

[99] B.K. Ridley, *Kinetics of radiative recombination in quantum wells,* Phys. Rev. B, **41**, 12190 (1990).

[100] S. Glasberg, H. Shtrikman and I. Bar-Joseph, *Optical Generation of spatially separated electron and hole gases in intrinsic GaAs/$Al_xGa_{1-x}As$ double quantum wells*, Phys. Rev. B, **63**, 113302 (2001).

[101] B.E. Kane, L.N. Pfeiffer and K.W. West, *Variable density of high mobility two dimensional electron and hole gases in a gated GaAs/AlGaAs heterostructure,* Appl. Phys. Lett., **63**, 2132 (1993).

[102] B.E. Kane *et al*., *Separately contacted electron-hole double layer in GaAs/AlGaAs heterostructure,* Appl. Phys. Lett., **65**, 3266 (1994).

[103] J. Yoon, C.C. Li, D. Shahar, D.C. Tsui and M. Shayegan, *Wigner Crystalization and Metal-Insulator Transition of Two-Dimensional Holes in GaAs at B=0,* Phys. Rev. Lett., **82**, 1744 (1999).

[104] M. Bugajski, W. Kuzko and K. Reginski, *Diamagnetic shift of exciton energy levels in GaAs/AlGaAs quantum wells,* Solid State Commun., **60**, 669 (1986).

[105] K.J. Nash, M.S. Skolnick, P.A. Claxton, J.S. Roberts, *Diamagnetism as a probe of exciton localization in quantum wells,* Phys. Rev. B, **39**, 10943 (1989).

[106] S. Ben Tabou de Leon and B. Laikhtman, *Exciton-exciton interactions in quantum wells : Optical properties, energy and spin relaxation,* Phys. Rev. B **,63,**125306, (2001).

[107] R. Zimmermann and C. Schindler, *Exciton-exciton interaction in coupled quantum wells* Solid State Comm., **144**, 395-398 (2007).

[108] C. Schindler and R. Zimmermann, *Analysis of the exciton-exciton interaction in semiconductor quantum wells*, Phys. Rev. B **78**, 045313 (2008).

[109] K.H. Gulden *et al.*, *Giant Ambipolar Diffusion Constant of n-i-p-i Doping Superlattices,* Phys. Rev. Lett., **66**, 373 (1991).

[110] M.B. Yairi and D.A.B. Miller, *Equivalence of diffusive conduction and giant ambipolar diffusion,* JAP, **91**, 4374 (2002).

[111] Y.N. Joglekar, A. V. Balatsky, M.P. Lilly, *Excitonic condensate and quasiparticle transport in electron-hole bilayer systems,* Phys. Rev. Lett., **72**, 205313 (2005).

5. List of Symbols

a_B	Bohr radius of excitons
B	Magnetic field
CQW	Coupled Quantum Well
d	Distance between the two quantum well centers
D_A	Ambipolar Diffusion coefficient
$D_{X,e,h}$	Diffusion coefficient of excitons, electrons and holes
e	Electronic charge
$e-h$	Electron-hole plasma
$E_{c,v}$	Energy of conduction, valence band edge
E_B	Exciton binding energies
E_g	Bandgap of semiconductor
E_{int}	Exciton-exciton interaction energy
E_L	Excitation laser energy
E_{lc}	Light cone energy
$f(T)$	Correlation factor
F	Applied Electric field
$F_{X,e-h}$	Free energy of the system below Mott transition, above Mott transition
I_{PL}	Photoluminescence intensity
IX	Indirect Exciton
$\hbar$	Plank's constant
k_B	Boltzmann's constant
l	Screening length
m_0	Rest mass of electron
$m_{e,hh,lh}$	Electron, heavy hole, light hole effective mass
M	Heavy hole exciton effective mass
$n_{X,IX}$	Density of direct excitons, indirect excitons
$n_{e,h}$	Density of electrons, holes
P	Excitation power of the laser

PL	Photoluminescence
QW	Quantum Well
Ry	Exciton Rydberg
$s_{e-h,X}$	Entropy per electron/hole , exciton
S	Rate of generation/annihilation of photoexcited carriers
t	Time
T	Temperature
X	Exciton
α	Spring constant
β	Electron hole recombination constant
$\gamma_{1,2}$	Luttinger parameters
Γ	Ratio of indirect and direct lifetimes
$\delta E(n)$	Density dependent energy shift
$\Delta E(B)$	Magnetic field dependent energy shift
ε	Dielectric Constant
η	Ratio of the photoluminescence intensities
$\varsigma_{e,h,X}$	Chemical potential of electrons, holes, excitons
λ	Variational Parameter
Λ	Diamagnetic coefficient
$\mu_{X,e,h}$	Mobility of excitons, electrons and holes
$\mu^{hh,lh}$	Reduced mass of heavy/light hole exciton
σ	Conductivity
Σ	Overlap integral
$\rho_{X,e,h}$	Density of states of excitons, electrons, holes
ρ	In-Plane relative coordinates
$\chi_{e/h,1/2}$	Ground state eigenfunctions of the electron/hole in narrow/wide quantum well
$\tau_{X,IX}$	Radiative lifetime of Exciton, Indirect Exciton
Ψ	Exciton wavefunction
Ω	Volume

6. Publications

- M. Stern, V. Garmider, V. Umansky and I. Bar-Joseph, *Mott transition of Excitons in Coupled Quantum Wells*, Phys. Rev. Lett., **100**, 256402 (2008).
- M. Stern, V. Garmider, E. Segre, M. Rappaport, V. Umansky, Y. Levinson and I. Bar-Joseph, *Photoluminescence ring formation in coupled quantum wells: excitonic versus ambipolar diffusion,* Phys. Rev. Lett., **101**, 257402 (2008).

Research Independence

This thesis summarizes my independent research conducted in the Weizmann Institute of Science.